



**HAL**  
open science

## **Dynamics of bidisperse suspensions under stokes flows: linear shear flow and eedimentation**

Micheline Abbas, Éric Climent, Olivier Simonin, Martin R. Maxey

► **To cite this version:**

Micheline Abbas, Éric Climent, Olivier Simonin, Martin R. Maxey. Dynamics of bidisperse suspensions under stokes flows: linear shear flow and eedimentation. *Physics of Fluids*, 2006, 1 (12), pp.121504/1-121504/20. 10.1063/1.2396916 . hal-03595571

**HAL Id: hal-03595571**

**<https://hal.science/hal-03595571>**

Submitted on 3 Mar 2022

**HAL** is a multi-disciplinary open access archive for the deposit and dissemination of scientific research documents, whether they are published or not. The documents may come from teaching and research institutions in France or abroad, or from public or private research centers.

L'archive ouverte pluridisciplinaire **HAL**, est destinée au dépôt et à la diffusion de documents scientifiques de niveau recherche, publiés ou non, émanant des établissements d'enseignement et de recherche français ou étrangers, des laboratoires publics ou privés.



## Open Archive Toulouse Archive Ouverte (OATAO)

OATAO is an open access repository that collects the work of Toulouse researchers and makes it freely available over the web where possible.

This is an author-deposited version published in: <http://oatao.univ-toulouse.fr/>  
Eprints ID : 2735

### **To link to this article :**

URL : <http://dx.doi.org/10.1063/1.2396916>

### **To cite this version :**

Abbas, Micheline and Climent, Eric and Simonin, Olivier and Maxey, M.R.  
(2006) *Dynamics of bidisperse suspensions under Stokes flows: Linear shear flow and Sedimentation*. *Physics of Fluids*, vol. 18 (n° 12). 121504/1-121504/20. ISSN 1070-6631

Any correspondence concerning this service should be sent to the repository administrator: [staff-oatao@inp-toulouse.fr](mailto:staff-oatao@inp-toulouse.fr)

# Dynamics of bidisperse suspensions under Stokes flows: Linear shear flow and sedimentation

Micheline Abbas and Eric Climent<sup>a)</sup>

*Laboratoire de Génie Chimique, UMR 5503 CNRS/INPT/UPS, 5 Rue Paulin Talabot, 31106 Toulouse, France*

Olivier Simonin

*Institut de Mécanique des Fluides, UMR 5503 CNRS/INPT/UPS, Avenue du Pr. Camille Soula, 31400 Toulouse, France*

Martin R. Maxey

*Division of Applied Mathematics, Brown University, Box F, Providence, Rhode Island 02912*

Sedimenting and sheared bidisperse homogeneous suspensions of non-Brownian particles are investigated by numerical simulations in the limit of vanishing small Reynolds number and negligible inertia of the particles. The numerical approach is based on the solution of the three-dimensional Stokes equations forced by the presence of the dispersed phase. Multibody hydrodynamic interactions are achieved by a low order multipole expansion of the velocity perturbation. The accuracy of the model is validated on analytic solutions of generic flow configurations involving a pair of particles. The first part of the paper aims at investigating the dynamics of monodisperse and bidisperse suspensions embedded in a linear shear flow. The macroscopic transport properties due to hydrodynamic and nonhydrodynamic interactions (short range repulsion force) show good agreement with previous theoretical and experimental works on homogeneous monodisperse particles. Increasing the volumetric concentration of the suspension leads to an enhancement of particle fluctuations and self-diffusion. The velocity fluctuation tensor scales linearly up to 15% concentration. Multibody interactions weaken the correlation of velocity fluctuations and lead to a diffusion-like motion of the particles. Probability density functions show a clear transition from Gaussian to exponential tails while the concentration decreases. The behavior of bidisperse suspensions is more complicated, since the respective amount of small and large particles modifies the overall response of the flow. Our simulations show that, for a given concentration of both species, when the size ratio  $\lambda$  varies from 1 to 2.5, the fluctuation level of the small particles is strongly enhanced. A similar trend is observed on the evolution of the shear induced self-diffusion coefficient. Thus, for a fixed  $\lambda$  and total concentration, increasing the respective volume fraction of large particles can double the velocity fluctuation of small particles. In the second part of the paper, the sedimentation of a single test particle embedded in a suspension of monodisperse particles allows the determination of basic hydrodynamic interactions involved in a bidisperse suspension. Good agreement is achieved when comparing the mean settling velocity and fluctuation levels of the test sphere with experiments. Two distinct behaviors are observed depending on the physical properties of the particle. The Lagrangian velocity autocorrelation function has a negative region when the test particle has a settling velocity twice as large as the reference velocity of the surrounding suspension. The test particle settles with a zig-zag vertical trajectory while a strong reduction of horizontal dispersion occurs. Then, several configurations of bidisperse settling suspensions are investigated. Mean velocity depends on the concentration of both species, density ratio and size ratio. Results are compared with theoretical predictions at low concentration and empirical correlations when the assumption of a dilute regime is no longer valid. For particular configurations, a segregation instability sets in. Columnar patterns tend to collect particles of the same species and eventually a complete separation of the suspension is observed. The instability threshold is compared with experiments in the case of suspensions of buoyant and heavy spheres. The basic features are well reproduced by the simulation model.

## I. INTRODUCTION

The precise understanding of the physics of suspended solid particles is assuming greater importance in industrial

applications, driven both by environmental issues and optimization of operating costs. Some industrial processes like water waste treatment, chemical and biorheological processes need models to predict the behavior of solid/liquid suspensions. We focus on two generic configurations of suspension flow: the batch sedimentation of particles in a qui-

<sup>a)</sup> Eric.Climent@ensiacet.fr

escent fluid, and suspensions where the fluid undergoes a simple shear. The sedimentation process is basically used for separating particle-laden fluid and the sheared suspensions are sites for migration (Ref. 1) and mixing of particles in various viscometric flows (blood, etc.). Even though such topics started to be studied at the beginning of the last century with experiments for Stokes flows, there are still some open issues related to the evolution of the microstructure in sedimentation, to the velocity fluctuations and dispersion of particles in a shear flow. We give special attention to bidisperse suspensions, because most industrial applications deal with highly nonuniform distributions of particle size or density and polydisperse suspensions have received much less attention than monodisperse ones. Our aim is to understand, in the limit of very small Reynolds and Stokes number, the microrheological and transport properties of nondilute bidisperse suspensions, where long range velocity perturbations generate intricate multibody interactions (see Ref. 2 for some illustrative flow configurations of a bidisperse suspension). We restrict our study to non-Brownian particles as the typical size is far beyond the colloidal limit. To answer basic questions that arise from industrial applications, it would be needed to predict the dynamics of suspensions and the role of the microstructure on the hydrodynamic interactions from a macroscopic point-of-view (the mean settling velocity, velocity fluctuations, spreading of interfaces, diffusion, stability and rheology of suspensions). This prediction is much more difficult in heterogeneous suspensions because the physical parameters that control the interactions are more numerous.

In the sedimentation case, the prediction of the mean settling velocity of the particulate phase can be provided by theoretical analysis (Ref. 3) or by empirical correlations (Refs. 4 and 5) based on numerous experiments. The agreement and the level of predictability are generally acceptable for most applications. When the suspension is statistically homogeneous, theoretical predictions (Refs. 6 and 7) exhibit a divergent increase of the fluctuation levels with the size of the vessel. Collective effects enhance the sedimentation velocity of particle clusters. As the width of the container becomes larger, the typical size of clusters increases and induces a high level of fluctuations. No experimental evidence (Ref. 8) supports this proposition and various screening mechanisms have been proposed (Refs. 9–11). The presence of walls can promote horizontal or vertical gradients of concentration (Refs. 12 and 13) acting as a sink of velocity fluctuations. Mucha *et al.*<sup>14</sup> provided new insights on the relation between the fluctuation level and a vertical gradient of concentration in the settling suspension. All the experiments are undoubtedly not homogenous and weak gradients of concentration can influence the overall dynamics of the flow suspension. In simulations, periodic boundaries induce strict conditions of homogeneity and so fluctuation levels tend to diverge in Stokes suspensions (Refs. 15–17). In the simulation of settling suspensions, when the presence of a bottom wall is imposed, saturation of the fluctuation levels is recovered as a vertical gradient of concentration develops (Ref. 18). But the controversy is still open while simulations with top and bottom walls do not exhibit any gradient of the

particulate concentration in the bulk but confirm that particle velocity fluctuations are strongly suppressed (Ref. 19). An important result of the recent work of Nguyen and Ladd<sup>19</sup> is that even a weak polydispersity of the particle size distribution can dramatically damp velocity fluctuations.

A bidisperse suspension can be characterized by four nondimensional parameters. The size ratio  $\lambda = a_2/a_1$ , the particulate concentrations of both species  $\phi_1, \phi_2$  (the total concentration of the suspension being  $\phi = \phi_1 + \phi_2$ ), and the ratio of reduced densities  $\gamma = \Delta\rho_2/\Delta\rho_1$  (where  $\Delta\rho$  is the density difference between the fluid and the particle  $\Delta\rho = \rho - \rho_f$ ). The index 1 is associated with small particles, and 2 with large particles. For a suspension settling under gravity, a useful combination of these parameters defines the ratio of the settling velocities:  $R_S = V_{o2}/V_{o1} = \gamma\lambda^2$  ( $V_o$  being the Stokes velocity of a single particle in an unbounded quiescent fluid).

Distinct approaches have been proposed to investigate the sedimentation in a polydisperse suspension. Theoretical predictions are based on the analytic solution of interactions between unequal spheres in the Stokes flow regime (Ref. 20). With an assumption of a homogeneous suspension, Batchelor and Wen<sup>21</sup> derived analytic expressions of the mean settling velocity in the dilute regime. A number of experiments (see Refs. 22–24) have verified that their results match quantitatively the theoretical predictions. Away from the dilute regime, most experiments are fitted by empirical relations but agreement between the results of distinct authors is generally qualitative. Davis and Gecol<sup>25</sup> proposed an interesting scaling relation without open parameters using the coefficients derived in the dilute regime. Peysson and Guazzelli<sup>26</sup> have recently investigated experimentally the evolution of the velocity fluctuations in a bidisperse suspension. Numerical simulations are also very instructive. Revay and Higdon<sup>27</sup> have proposed simulations devoted to concentrated configurations. They are based on the solution of Stokes equations accounting for lubrication effects for the near-field interaction. They formed averages over different spatial microstructures achieved by random seeding of the particles. In their study, particle velocities are related to only static interactions as the trajectories are not computed. Da Cunha *et al.*<sup>28</sup> have also proposed some new results on dynamic interactions in monodisperse and polydisperse particulate Stokes flows. They compared their results obtained with ordered and random particle positions with theories and experiments. They found good agreement for moderately concentrated suspensions. Nevertheless, simulations on this topic are still very few and it is still a challenging task to model the dynamic behavior of complex dispersed two-phase flows.

When the flow is not driven by particles settling under gravity, particle interactions are due to velocity gradients in the carrying flow. Less theoretical and experimental works exist on polydisperse suspensions under shear flow. Batchelor and Green<sup>29</sup> have analytically determined the hydrodynamic interactions between a pair of particles. More recently, Drazer *et al.*<sup>30</sup> have calculated translational and rotational velocity fluctuations from low to high concentrated, homogeneous monodisperse suspensions. Although the Stokesian dynamics method they used gives an accurate solution of the Stokes equations, the authors were limited to simulating the

simultaneous motion of a few hundred particles because of CPU limitations. They have found that the fluctuations resulting from dynamic interactions in a shear flow are higher than those resulting from a frozen random microstructure of the suspension. But in both cases, the fluctuation level follows the dilute limit estimation based on pairwise interactions up to 15% volume concentration. In a former work, Drazer *et al.*<sup>31</sup> showed that the probability distribution function of the velocity fluctuations have an exponential shape at low concentrations as a signature of long term correlated structures. They appeared to be Gaussian at high concentrations where hydrodynamic screening is achieved by the random multibody interactions. Lagrangian velocity autocorrelation functions computed by Marchioro and Acrivos<sup>32</sup> and Drazer *et al.*<sup>31</sup> decay with time, change over to negative values starting from a characteristic time scale of order  $1/G$  (where  $G$  is the flow shear rate) then go through a minimum before approaching zero from below. This scaling shows that particle trajectories are basically controlled by pair encounters at low concentration. The velocity fluctuations induce after a long time a chaotic evolution of the suspension, which is known to lead to the shear induced self-diffusion of particles even in the absence of a gradient of concentration and for uniform shear. The diffusion process exists with only hydrodynamics, even when Brownian thermal agitation is negligible (infinite Péclet number and no inertia). Diffusion coefficients are strongly increasing with the suspension concentration. Diffusion in such conditions has been studied in many works, from the reference work of Leighton and Acrivos<sup>33</sup> to new experimental techniques developed by Breedveld *et al.*<sup>34–36</sup> and numerical simulations of Marchioro and Acrivos,<sup>32</sup> Drazer *et al.*,<sup>31</sup> Sierou and Brady.<sup>37</sup> Their results match only qualitatively because of experimental uncertainties and simulation shortcomings. The statistical behavior of polydisperse sheared suspensions has not been thoroughly explored. Chang and Powell<sup>38,39</sup> have studied the influence of bimodal particles on the microstructure organization in nearly close-packing suspensions. They also addressed the determination of the suspension viscosity as well as the short time and long time diffusivity.

Sedimentation and shear induced migration may exist simultaneously when settled particles are exposed to a shear flow. Nonhomogeneity of the particle distribution and variation of the effective viscosity induce the particle migration across the streamlines of the flow. Viscous resuspension has an important effect on the dynamic response of the suspension in complex flows. Migration of particles is related to several mechanisms: gradient of shear, gradient of concentration, and curvature of the streamlines. The behavior of polydisperse systems is more complex than that observed in the monodisperse system. Shauly *et al.*<sup>40,41</sup> have proposed models extended to polydisperse systems and they were able to compare their results favorably with experimental steady profiles of particle concentration.

A fully coupled numerical model allows us to simulate several configurations of bidisperse settling and sheared suspensions. Under the approximation of Stokes flow, the model is able to simulate dynamic interactions between thousands of particles. The paper is organized as follows: First, we

briefly describe the numerical model and reference previous validations and studies. Then, we proposed validations of the numerical approach for the special case of unequal particles. The paper aims at investigating settling suspensions and shear induced interactions. We address the determination of statistical quantities of monodisperse and bidisperse solid-liquid sheared suspensions. We have a special interest in the simple case of a settling test sphere embedded in a monodisperse suspension. Finally, we investigate the particular behavior of suspensions undergoing a drastic segregation process as observed by Weiland *et al.*<sup>42</sup> and Batchelor and Van Rensburg.<sup>43</sup>

## II. NUMERICAL MODEL AND VALIDATION

The complexity of dispersed two-phase flows is related to the numerous length scales that have to be resolved simultaneously. In the case of Stokes flows, the velocity disturbance induced by a single particle falls off very slowly and then multibody hydrodynamic interactions control the evolution of the suspension. Stokesian dynamic (Ref. 44) simulations have been extensively used to model the behavior of colloidal and noncolloidal systems under the low Reynolds number assumption. They require the inversion of the mobility matrix and are limited to a few hundred particles. A number of improvements have been proposed to reduce the computational cost of the initial technique (splitting the hydrodynamic interactions into a far-field mobility calculation and a pairwise additive resistance interaction, see Ref. 45). The major step forward is probably the accelerated Stokesian dynamics proposed by Sierou and Brady.<sup>46</sup> It is now possible to simulate hydrodynamic interactions among  $O(10^3)$  particles. Other numerical methods have been successfully used outside the Stokes regime (distributed Lagrangian multiplier,<sup>47</sup> front tracking method<sup>48</sup>).

We propose to use a numerical model, which is able to simultaneously couple the solution of fluid flow equations and the Lagrangian tracking of the particles. The force coupling method (FCM) is based on a low order multipole expansion of the velocity disturbance induced by the presence of particles. The equations of the fluid motion are solved directly and the forcing term is modeled by a spatial source of momentum added to the Stokes equations. The accuracy of the model increases as we add higher order terms in the multipole expansion, but solving the equations becomes more time consuming.

### A. Model equations

We consider that the fluid is incompressible [Eq. (1)], we neglect the inertia of the fluid and assume a constant viscosity  $\mu$  for the carrying fluid flow. The velocity field  $\mathbf{u}(\mathbf{x}, t)$  and the pressure  $p(\mathbf{x}, t)$  are solutions of the Stokes equations [Eqs. (1) and (2)],

$$\nabla \cdot \mathbf{u} = 0, \quad (1)$$

$$\mathbf{0} = -\nabla p + \mu \nabla^2 \mathbf{u} + \mathbf{f}(\mathbf{x}, t). \quad (2)$$

The forcing term on the right-hand side of Eq. (2) is a spatial distribution of momentum which is induced by the presence

of the moving particles. This term is spatially and temporally evolving while the particles are freely moving under hydrodynamic interactions. Its expression is based on the theoretical analysis of low Reynolds number flows. We consider only two terms [see Eq. (3)] of the multipole expansion, namely the force monopole (Stokeslet) and the force dipole,

$$f_i(\mathbf{x}, t) = \sum_{n=1}^{N_B} \left[ F_i^{(n)} \Delta(\mathbf{x} - \mathbf{Y}^{(n)}(t)) + G_{ij}^{(n)} \frac{\partial}{\partial x_j} \Delta'(\mathbf{x} - \mathbf{Y}^{(n)}(t)) \right]. \quad (3)$$

The  $N_B$  particles are centered at locations  $\mathbf{Y}^{(n)}(t)$  and the source terms are spread out on the flow field using finite size envelopes [Eq. (4)]. The width of the Gaussian envelopes [ $\sigma$  for  $\Delta(x)$  and  $\sigma'$  for  $\Delta'(x)$ , respectively] are related to the particle radius  $a$  by analytic expressions

$$\Delta(\mathbf{x}) = (2\pi\sigma^2)^{-3/2} e^{-(r^2/2\sigma^2)} \quad \text{with } r = |\mathbf{x}|. \quad (4)$$

The magnitude of the interaction force  $\mathbf{F}^{(n)}$  is directly related to the force acting on the considered particle. It is a combination of buoyancy, inertia effect, and an external force  $\mathbf{F}_{\text{ext}}$  [Eq. (5)],

$$\mathbf{F}^{(n)} = (m_P - m_F) \left( \mathbf{g} - \frac{d\mathbf{V}^{(n)}}{dt} \right) + \mathbf{F}_{\text{ext}}, \quad (5)$$

$\mathbf{G}_{ij}^{(n)}$  is a tensor which can be split into symmetric and anti-symmetric parts. The symmetric part (namely, the stresslet) contributes to enforce a solid body rotation within the fluid occupied by the particle,

$$\mathbf{T}^{(n)} = - (I_P - I_F) \left( \frac{d\mathbf{\Omega}^{(n)}}{dt} \right) + \mathbf{T}_{\text{ext}}. \quad (6)$$

Similarly the torque term [Eq. (6)] sets the amplitude of the antisymmetric part of  $G_{ij}^{(n)}$ ,  $m_P$  (respectively,  $m_F$ ) is the mass of the particle (respectively, fluid) volume and  $I_P$  (respectively,  $I_F$ ) is the particle (respectively, fluid) rotational inertia. Throughout the paper, both the translational and rotational inertia of particles will be neglected. The ratios  $a/\sigma$  and  $a/\sigma'$  are set as to match, respectively, the Stokes drag for an isolated sphere (radius  $a$ ) and to ensure an average zero rate of strain [Eq. (7)] within the volume occupied by the particle,

$$S_{ij} = \frac{1}{2} \int \left( \frac{\partial u_i}{\partial x_j} + \frac{\partial u_j}{\partial x_i} \right) \Delta'(\mathbf{x} - \mathbf{Y}^{(n)}(t)) d^3\mathbf{x} = 0. \quad (7)$$

These requirements are fulfilled exactly in the limit of the Stokes approximation while  $a/\sigma$  and  $a/\sigma'$  are set analytically for a Gaussian shaped envelope:  $a/\sigma = \sqrt{\pi}$  and  $a/\sigma' = (6\sqrt{\pi})^{1/3}$  (see details in Refs. 49 and 50).

Our paper aims at investigating two flow configurations where each term has a special contribution. The sedimentation process is basically controlled by particles settling under gravity. Hindrance effects are mostly due to the backflow of the continuous phase but also to other factors such as the effective viscosity of the suspension. The FCM includes both contributions. The force monopole term is dominant driving

the interphase coupling mechanisms for settling suspensions and the effective viscosity enhancement is also modeled through the contribution of stresslets. When the suspension is embedded in a shear flow, the force monopole is negligible and the stresslet will be the major contribution for nonbuoyant spheres.

Particles move freely in a Lagrangian framework as their trajectory equations are solved simultaneously. Particle velocities and rotation rates are obtained with a spatial filtering of the flow velocity field based on the spherical Gaussian envelopes [Eqs. (8) and (9)],

$$\mathbf{V}^{(n)}(t) = \int \mathbf{u}(\mathbf{x}, t) \Delta(\mathbf{x} - \mathbf{Y}^{(n)}(t)) d^3\mathbf{x}, \quad (8)$$

$$\mathbf{\Omega}^{(n)}(t) = \int \nabla \times \mathbf{u}(\mathbf{x}, t) \Delta(\mathbf{x} - \mathbf{Y}^{(n)}(t)) d^3\mathbf{x}. \quad (9)$$

Then, the trajectory of each particle is computed by integrating Eq. (10),

$$\frac{d\mathbf{Y}^{(n)}}{dt} = \mathbf{V}^{(n)}(t). \quad (10)$$

Time evolution is performed by means of a fourth order Adams-Bashforth scheme. Periodic boundary conditions are imposed on the simulation domain for modeling the evolution of a random homogeneous suspension. The numerical scheme used for the solution of the Stokes equations takes advantage of the periodic boundary conditions by using fast Fourier transforms. We used a method of domain decomposition to achieve scalable performance on parallel supercomputers. The width of the cubic domain  $L$  is kept constant and equal to  $2\pi$ . Various volumetric concentrations of the suspension correspond to the different number of particles in the domain, typically 3200 particles for a 12% concentration in a  $128^3$  domain. More details on the theoretical background and an extensive validation of the method are available in Refs. 49–51.

## B. Validation tests

Results on both sedimenting and sheared suspensions of solid particles can be obtained by means of two distinct procedures because Stokes equations are not time dependent and the velocity field depends only on the relative positions of the particles. In a static simulation, particles are randomly seeded in the domain and the computation of interactions provides the flow velocity distribution and consequently the particle velocities. Particle seeding respect the nonoverlapping condition. Averages over several seeding (random microstructure) are formed to get statistical quantities. The dynamic way to form averages accounts for the unsteady evolution of the suspension. Particles are initially seeded at random positions. Then, trajectories are computed as a following sequence of fully coupled interactions between the fluid and the particles. Ensemble averages are formed over all the particles as time goes on. In the case of settling spheres in an initially quiescent fluid, the back flow hinders the mean velocity of the suspension. A uniform upward pressure gradient counterbalances the average forcing term in-

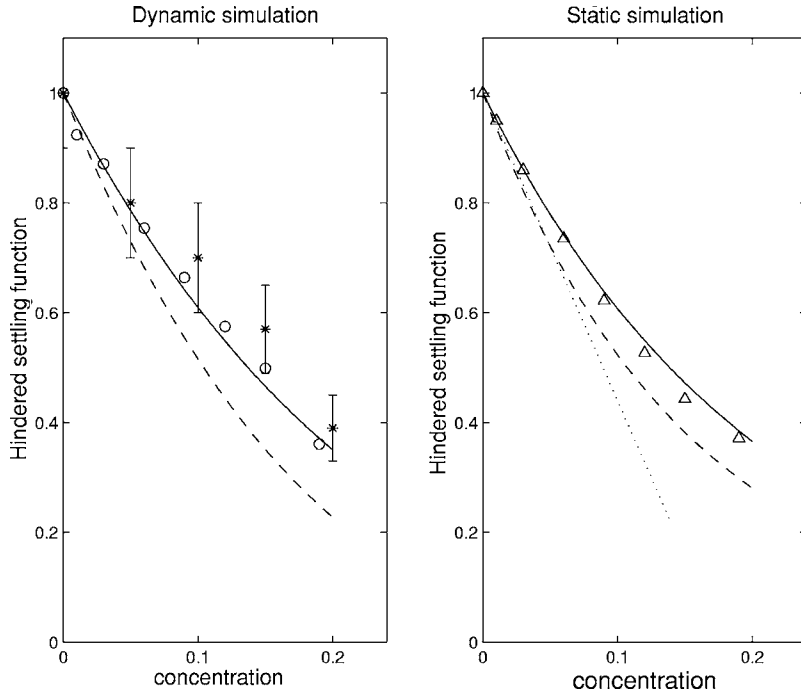


FIG. 1. Mean settling velocity of a monodisperse suspension. Left: Richardson and Zaki (Ref. 4) ( $n=4.7$ , solid line), Buscall *et al.* (Ref. 5) (dashed line), FCM simulation (circles), Nicolai *et al.* (Ref. 66) (stars). Right: Batchelor (Ref. 3) (dotted line), Brady and Durlofsky (Ref. 72) (solid line), Revay and Higdon (Ref. 27) (dashed line), FCM simulation (triangles).

duced by buoyancy forces of settling particles. We compare the results of the two averaging procedures in Fig. 1 when the suspension is monodisperse. It is clear that, our simulations with the FCM lies within the error bars of the careful experiments of Nicolai *et al.*<sup>52</sup> and are well approximated by classic empirical relations. We observed that both the static and dynamic simulations are close to other studies. The mean settling rate of a suspension is not a suitable quantity to validate the adequacy of the model as error bars of experiments and assumptions of theories restrict the precision of the results. For more details on the simulation of monodisperse settling suspensions, we refer to our former work (Ref. 17) where we focused on inertial screening in low-but-finite Reynolds number sedimentation.

In previous studies, the FCM has been validated only for particles of equal size. In the present paper, we present careful comparisons with analytic solutions of the flow around sedimenting particles of unequal size and density (Ref. 53). In Fig. 2, the relative velocity of particles aligned vertically or horizontally shows an excellent agreement for the resolution of the far field flow  $U_{12}$  and  $V_{12}$  characterize the relative velocities of two settling particles aligned vertically and horizontally. In the reference case of equal spheres, both quantities are identically equal to zero as particles settle with the same velocity for any separation distance. Remember that  $\lambda=a_2/a_1$  is the size ratio (the index 1 is associated with the small particle and 2 with the large one) and  $\gamma = \Delta\rho_2/\Delta\rho_1$  is the reduced density ratio. With the monopole

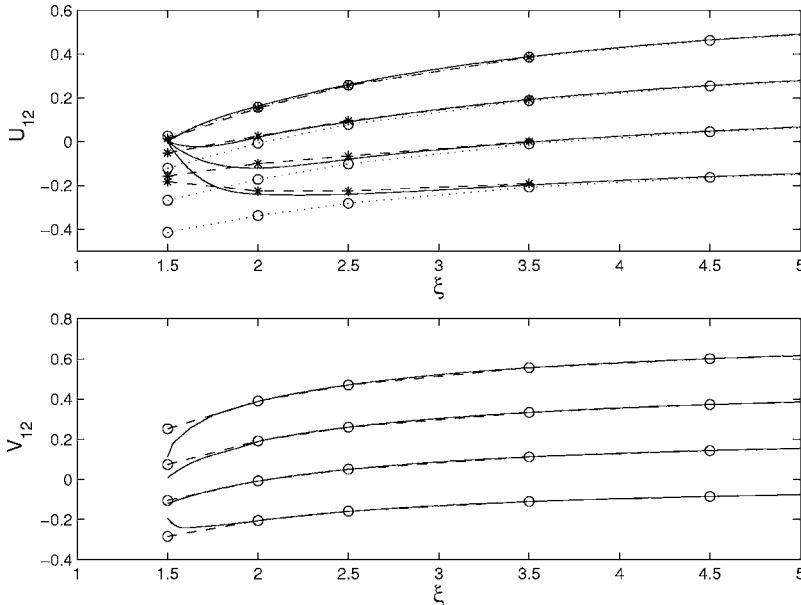


FIG. 2. Relative settling velocity of two isolated unequal spheres ( $\lambda=2$  and  $\gamma=1; 1/2; 1/3; 1/4$ ; from top to bottom).  $U_{12}$ : particles are aligned vertically;  $V_{12}$ : particles are aligned horizontally. Solid line: analytic solution (Wacholder and Sather, Ref. 53); dashed line and circles: FCM monopole; dashed line and stars: FCM monopole and dipole.

only, the model is clearly less accurate in the configuration of vertically aligned particles. The flow perturbation induced by the upper particle has to flow around the other particle. In the FCM, fluid fills the entire domain and particles do not have a physical solid-liquid interface. When the gap  $\xi=r/a_2$  is smaller than 2.5 ( $\xi=1.5$  corresponds to contact for  $\lambda=2$ ) the discrepancy becomes important. The multipole decomposition truncated to the first order (force monopole) is not sufficient when near field interactions have to be accounted for. Therefore, we have to improve the flow resolution by incrementing the order of the multipole decomposition. The precision of the FCM is increased by adding the force dipole in the source term. An iterative scheme is used to enforce a zero rate of strain within the volume occupied by the particles. In Fig. 2 (top), we point out that including the force dipole provides a net benefit on the resolution of short range interactions. With a set of particular parameters, unusual closed trajectories develop (Ref. 53). We obtained the same orbital trajectories but when particles are close to contact our model is unable to reproduce lubrication effects within the thin gap. In the case of sedimenting particles, close contact of particles are not expected to occur very often and dynamics is related to collective hydrodynamic interactions.

Particles suspended in a shear flow are driven continuously by the flow and approach each other along the compression axis. In the case of neutrally buoyant particles, the interaction is driven only by the symmetric force dipole. We used the FCM for the case of a pair of interacting particles in a shear flow, and the results were compared to the study of Batchelor and Green<sup>29</sup> who have determined analytical expressions of the relative velocity [Eq. (11)] and rotation rate [Eq. (12)]. These expressions can be written in terms of three nondimensional functions (A, B, and C) which depend on the particle nondimensional separation distance  $r/a$ ,

$$\mathbf{V}(r) = -G \begin{cases} r_2(B/2 + r_1^2/r^2(A-B)), \\ r_1(B/2 + r_2^2/r^2(A-B)), \\ r_1 r_2 r_3 / r^2 (A-B), \end{cases} \quad (11)$$

$$\mathbf{\Omega}(r) = -\frac{CG}{2} \begin{cases} r_1 r_3 / r^2, \\ -r_2 r_3 / r^2, \\ (r_2^2 - r_1^2) / r^2, \end{cases} \quad (12)$$

$\mathbf{r}=(r_1, r_2, r_3)$  is the separation distance between the two particle centers and  $G$  is the shear rate of the flow. The direction 1 is the mean flow direction, 2 is the direction of shear and direction 3 is normal to the plane of shear (vorticity direction). The evolutions of A, B, and C are plotted in Figs. 3(a) and 3(b) for two equal or unequal particles. Precise values of A and B in the case of unequal particles were obtained by Pesche.<sup>54</sup> It is clear that the FCM performs well when the distances between solid boundaries are sufficiently large, but it does not capture the local effects of viscous lubrication forces for small gap widths. To improve the results, Dance and Maxey<sup>55</sup> developed a parameterization of the lubrication forces to achieve a better accuracy of short-range hydrodynamic interactions. Their work was based on exact results for isolated pairs of equal particles, and on careful cross-checking of results published in the literature. Lubrication

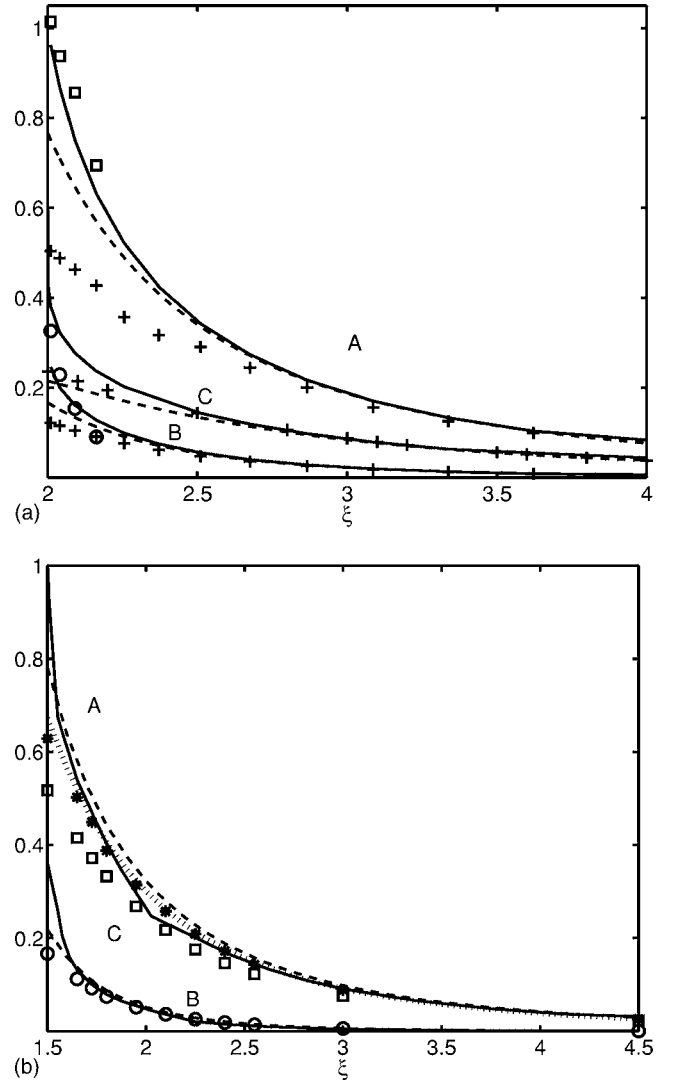


FIG. 3. A, B, and C vs the separation distance  $\xi=r/a_2$ . Solid lines: analytical solution [(a) Batchelor and Green, Ref. 29 and (b) Pesche, Ref. 54]. Dashed lines: far-field approximation (Batchelor and Green, Ref. 29 in both figures). Symbols are from this work: (a)  $\lambda=1$ : Plus: A, B and C with FCM alone; open squares and circles: A and B with [FCM + lubrication forces ( $\xi \leq 2.2$ )]. (b)  $\lambda=2$ : squares: A, circles: B, stars: C, dotted line: far-field approximation of C.

forces are calculated in a pairwise additive manner. Figure 3(a) shows that the calculation of the interactions between close particles is significantly improved when the lubrication forces are added to the FCM. These forces were applied for dimensionless gap widths between particle surfaces  $\varepsilon=(r/a)-2 \leq 0.2$ , since the force components were determined using asymptotic expansions.

### C. Nonhydrodynamic repulsive force

Obviously, the FCM is only an approximate model since fluid occupies the whole domain and no-slip boundary conditions on the particle surface are not strictly imposed. Shear flow drives interacting particles in very close proximity. At short separation distance, the FCM is supplemented by the lubrication forces which become dominant. However, for a fixed time step, the hydrodynamic effects alone are not suf-



efficient to prevent particle numerical overlapping in all cases. Dratler and Schowalter<sup>56</sup> have found that even when the time step is drastically reduced and when the numerical stability problems are eliminated, particles still overlap with a minimum of 1 pair over 25 particles for moderate concentrations (less than 20%). The number of overlapping pairs increases with the concentration. Therefore we used a repulsion barrier. The repulsive force  $\mathbf{F}_b$  [Eq. (13)] is added to the monopole coupling term when the distance between the particle centers  $r$  is less than a prescribed cutoff separation distance  $R_{\text{ref}}$ ,

$$\mathbf{F}_b = -\frac{F_{\text{ref}}}{2a} \left[ \frac{R_{\text{ref}}^2 - r^2}{R_{\text{ref}}^2 - 4a^2} \right]^2 \mathbf{x}, \quad (13)$$

$\mathbf{F}_b$  is enabled at an activation distance corresponding to 10% of the particle radius when the repulsion barrier is used alone and 2.5% when it is supplemented to the lubrication forces. The profile of the force barrier varies smoothly from 0 to  $F_{\text{ref}}$  at contact. The force scale  $F_{\text{ref}}$  is calibrated to prevent overlapping of approaching particles. For any value of  $F_{\text{ref}}$  higher than the limit which prevents overlapping or for large variations of the activation distance (from 0.01  $a$  to 0.1  $a$ ) we did not observe significant variations (less than 10%) on the suspension statistics (velocity fluctuations and probability density functions) in the case of sheared suspensions. The determination of self-diffusion coefficients is more critical. This issue is discussed in Sec. III A. In the case of sedimenting suspensions, previous studies have also shown that the influence of the repulsive force on the overall dynamics of the suspension is not significant (Refs. 57 and 58). This rough treatment of the near-field hydrodynamics of particles near contact in both sheared and sedimenting configurations may restrict the accuracy of the model. Only low to moderately concentrated suspensions could be investigated (volumetric concentration lower than 20%).

Although this force is used to fix a numerical inaccuracy of the model by preventing particles from overlapping, it could be interpreted in terms of physical considerations. Even if particles in solid-liquid suspensions are not charged they generally experience a short range interparticle force due to electric-double layer repulsion (DLVO-type) when the gap is shorter than  $10^{-2} a$ . The suspensions that we study may be considered as stabilized suspensions while a strong repulsive force prevent the formation of permanent cluster of particles. Short range attraction forces such as the Van der Waals potential are screened by the hydrodynamic lubrication force and the repulsive barrier. The physical analog of our simulations would be the case where electrostatic repulsive forces are overcoming the Van der Waals attraction force.

We studied the role of the different contributions of FCM on the relative trajectories of two particles in a shear flow (Fig. 4). The particles are driven continuously to approach each other. The limit region of overlapping is materialized by the thin dashed line located at  $r=2a$ . The particles overlap when only the monopole and the dipole forces are applied. When the model is supplemented with the lubrication forces (nondimensional gap width  $\varepsilon \leq 0.2$ ), the ap-

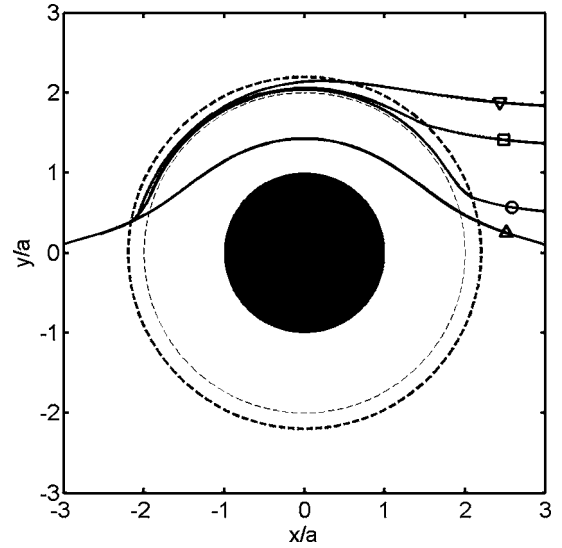


FIG. 4. Relative trajectory of the centers of two equal spheres in a shear flow [the initial relative position is  $(r_1=x=-3a; r_2=y=0.1a)$ ]. Filled circle: reference particle. Thin dashed circle:  $r/a=2$  (overlapping limit). Bold dashed line:  $r/a=2.2$  (limit of the lubrication layer).  $\Delta$ : FCM alone (monopole + dipole).  $\circ$ : [monopole + dipole + lubrication force ( $\varepsilon \leq 0.2$ )].  $\square$ : [monopole + dipole + repulsion force ( $\varepsilon \leq 0.05$ ) + lubrication force ( $\varepsilon \leq 0.2$ )].  $\nabla$ : [monopole + dipole + repulsion force ( $\varepsilon \leq 0.2$ )].

proaching particle rolls over the reference particle. The lubrication effects between close particles enhance the repulsive behavior on the approaching side and attraction on the receding side. In some cases, overlapping does occur and we need to include the repulsive barrier. Consequently, the fore-aft symmetry of the trajectory is broken and a finite drift characterizes the motion of the particles across the streamlines. If the repulsion force is used without the lubrication model, the finite drift is larger.

We point out that most of the results of monodisperse and bidisperse sheared suspensions were obtained using only the repulsion force within the FCM. Some specific simulations have been carried out with the lubrication model. In these cases, the local hydrodynamic interactions are properly modeled. Quantitative comparisons provide an evaluation of the accuracy of statistic quantities obtained with the repulsion force only.

### III. SUSPENSIONS IN A SIMPLE SHEAR

All the sheared suspensions considered in the present paper are macroscopically homogeneous, with neutrally buoyant, non-inertial and non-Brownian particles, in the limit of vanishing Reynolds number. In order to preserve the homogeneity of the suspension under shear flow, we impose periodic boundary conditions in the three directions. The Stokes equations are linear, so we only solve the perturbation of the flow induced by the presence of the particles (stresslet contributions) and superimpose a linear shear flow  $u_1=Gx_2$  ( $G$  is the shear rate) on the particle motions. When a particle exits the simulation domain from the bottom (respectively, upper) boundary, it appears on the opposite side, and its velocity must be adjusted by adding (respectively, removing) the flow velocity  $GL$ , where  $L$  is the typical width of the

domain (most simulations have been carried out with  $L/a = 48$ ). This is equivalent to applying the shear in a dynamic way by means of the Lees-Edwards boundary conditions (Ref. 59). In a sheared suspension the typical length, time and velocity scales are  $a$ ,  $G^{-1}$ , and  $aG$ , where  $a$  is the particle radius. The trajectories are integrated with a constant time step  $5 \times 10^{-3} G^{-1}$ . This corresponds to a decrement of  $a/100$  of the separation distance between two approaching particles. Statistical quantities are averaged over long time series. Typically, we simulate the suspension flow during a dimensionless time  $Gt$  proportional to  $100\phi^{-1/3}$ . During this time, a particle is expected to experience enough interactions with other particles to achieve its steady statistical regime. It has been clearly pointed out that the determination of self-diffusion coefficients needs very long time series for reaching the diffusive behavior (Ref. 37).

### A. Monodisperse suspensions

Based on the analytic expressions of the relative velocity of particle pairs in a Stokes shear flow, Batchelor and Green<sup>29</sup> have theoretically calculated the particle trajectories and the pair probability density function [namely,  $g(r)$  being its radial profile]. They showed that closed trajectories exist and produce a divergent evolution of  $g(r)$  at short separation distances. Stokes equations are linear and reversible. So a particle follows the same streamline before and after a particle encounter. Self-diffusion occurs due to an interaction with a third particle (Ref. 60) and more generally due to multibody hydrodynamic interactions. Acrivos *et al.*<sup>61</sup> studied the self-diffusion coefficient parallel to the flow by introducing a mechanism of an interaction with an additional pair of particles. A nonhydrodynamic repulsive force (electric double-layer repulsion, short scale roughness) leads to fore-aft symmetry breaking and a particle encounter induces a finite drift of the particles across the streamlines (Ref. 58) which also contributes to the diffusion of the particles. Using the analytic work of Batchelor and Green,<sup>29</sup> Drazer *et al.*<sup>30</sup> have predicted theoretically the evolution of the fluctuation (translation and rotation) tensors [Eqs. (14) and (15)] of the suspension. They used two approximations of the microstructure in the dilute limit, a purely random pair probability density function and the pair probability density function derived by Batchelor and Green<sup>29</sup> accounting for hydrodynamic interactions. Following symmetry arguments in a dilute suspension, the two diagonal terms  $T_{11}$  and  $T_{22}$  of the fluctuation tensor are equal. The nondiagonal terms are strictly zero when the fore-aft symmetry is preserved,

$$T_{ij} = (\langle v_i v_j \rangle - \langle v_i \rangle \langle v_j \rangle) / (Ga)^2, \quad (14)$$

$$w_{ij} = (\langle \Gamma_i \Gamma_j \rangle - \langle \Gamma_i \rangle \langle \Gamma_j \rangle) / (G)^2. \quad (15)$$

In Eqs. (14) and (15),  $v$  (respectively,  $\Gamma$ ) is the translational (respectively, rotation) particle velocity perturbation (the difference between the instantaneous velocity of the particle  $\mathbf{V}$  and the local nondisturbed fluid velocity  $\mathbf{u}$ ).  $\langle \rangle$  stands for averages in time and over all the particles. We verified that  $\langle v_i \rangle$  and  $\langle \Gamma_i \rangle$  are vanishingly small when averages are formed over long time series.

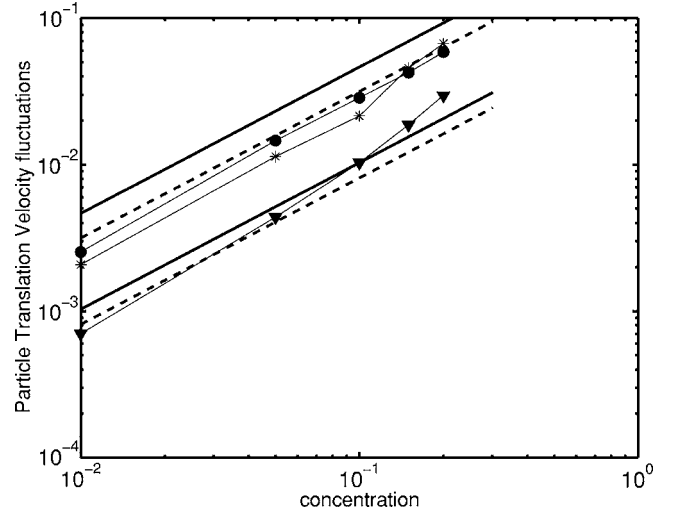


FIG. 5. Diagonal terms of the velocity fluctuation tensor vs concentration. Stars:  $T_{11}$ ; filled circles:  $T_{22}$ ; filled triangles:  $T_{33}$ ; solid lines: dilute limit theory based on the pair probability function of Batchelor and Green (Ref. 29). Dashed lines: dilute limit theory assuming a random distribution in a static simulation ( $T_{11} = T_{22} > T_{33}$ ).

Figure 5 shows that the diagonal terms of the translational velocity fluctuation tensor scale linearly with the concentration up to 20%. They are highly anisotropic, the fluctuations in the flow and shear directions ( $T_{11}$  and  $T_{22}$ ) are nearly four times larger than the fluctuations in the spanwise direction  $T_{33}$ . The velocity fluctuations of the particles are compared to the theoretical prediction of Drazer *et al.*<sup>30</sup> and show good agreement. A linear scaling was expected to occur up to moderately concentrated suspension as the velocity perturbations induced by the stresslet contribution decays like  $1/r^2$ . While the theoretical prediction of the absence of nondiagonal terms is based on an assumption of fore-aft symmetry of interactions, it is expected that adding a nonhydrodynamic repulsive force may induce a finite value of the  $T_{12}$  term. Figure 6 shows that all the nondiagonal terms are zero except  $T_{12}$  which is negative. Similarly, Drazer *et al.*<sup>30</sup>

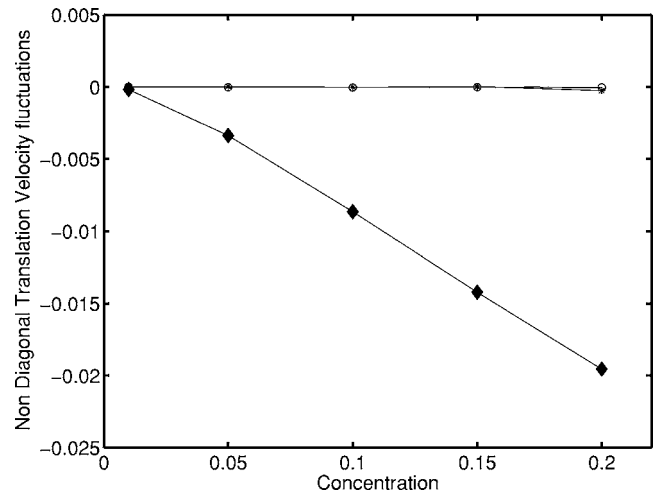


FIG. 6. Off-diagonal terms of the particle velocity fluctuation tensor vs concentration. Filled diamonds with solid line:  $T_{12}$ ; other symbols stand for  $T_{13}$  and  $T_{23}$ .

found that the magnitude of  $T_{12}$  increases with the concentration. The repulsive force depletes the receding side of the particles and then negative cross-products  $v_1 v_2$  of the velocity perturbations are more probable [see Eq. (11)]. Calculating the pair probability density function indicated that the radial dependence is not isotropic. The radial evolution shows a sharp peak at a separation distance near  $r=2a$  corresponding to contact. We have also noticed that the probability of finding close particle pairs in a shear suspension is larger than the peak value due to only excluded volume in a random static suspension. It suggests that hydrodynamic interactions under a shear flow increase the lifetime of particle pairs close to contact. Rotational fluctuation levels are not displayed but their evolution with increasing concentration followed a similar trend as discussed above. The fluctuations in the spanwise direction have the largest amplitude and  $w_{12}$  is positive and increases with the concentration.

When the numerical model is supplemented with the short-range lubrication forces, the fluctuation level is slightly higher (approaching the theoretical prediction in the dilute limit). Enhancement of velocity fluctuations by lubrication effects are related to an extended time of interacting particles in close vicinity.

Normalized probability density functions of the translational velocity fluctuations in the shear direction are shown in Fig. 7(a) for four different volume fractions. We obtained basically the same plots in other directions. The first observation is that the shape is changing as the concentration increases. Intense velocity fluctuations are more probable than the Gaussian estimate. For example, in Fig. 7(b) (5% concentration), a best fit show of the pdf is composed of a Gaussian behavior for the weak velocity fluctuations  $|v/s| < 1$  (where  $s$  is the standard deviation of velocity fluctuations) and exponential tails for intense fluctuations. Such a statistical behavior is related to the presence of persistent small-scale structures, due presumably to the short range hydrodynamic interactions of pair of particles at low volume fraction (Ref. 31). Simulations including the lubrication forces gave very similar results. Whereas, when the concentration is increased, the probability density function has a more pronounced Gaussian shape. The mean separation distance between the particles is reduced leading to multiple many-body interactions with a weaker overall correlation.

The time required to get uncorrelated velocity fluctuations along the particle trajectories is characterized by the evolution of the normalized Lagrangian velocity autocorrelation function  $R_{22}(t)$  in the transverse direction. Figure 8 is a plot of the velocity autocorrelation functions for different suspension volumetric concentrations up to 20%. It can be observed that in all cases the velocity fluctuations change their sign after a typical time of order  $1/G$  suggesting that pairwise interaction is the major contribution to anticorrelated motions. A two particle encounter has a lifetime of  $1/G$ . The negative region is more pronounced at low concentration but is still prominent at moderate concentration in agreement with Marchioro and Acrivos.<sup>32</sup> Another important characteristic time scale is the time required to reach uncorrelated fluctuations. We obtained that fully uncorrelated mo-

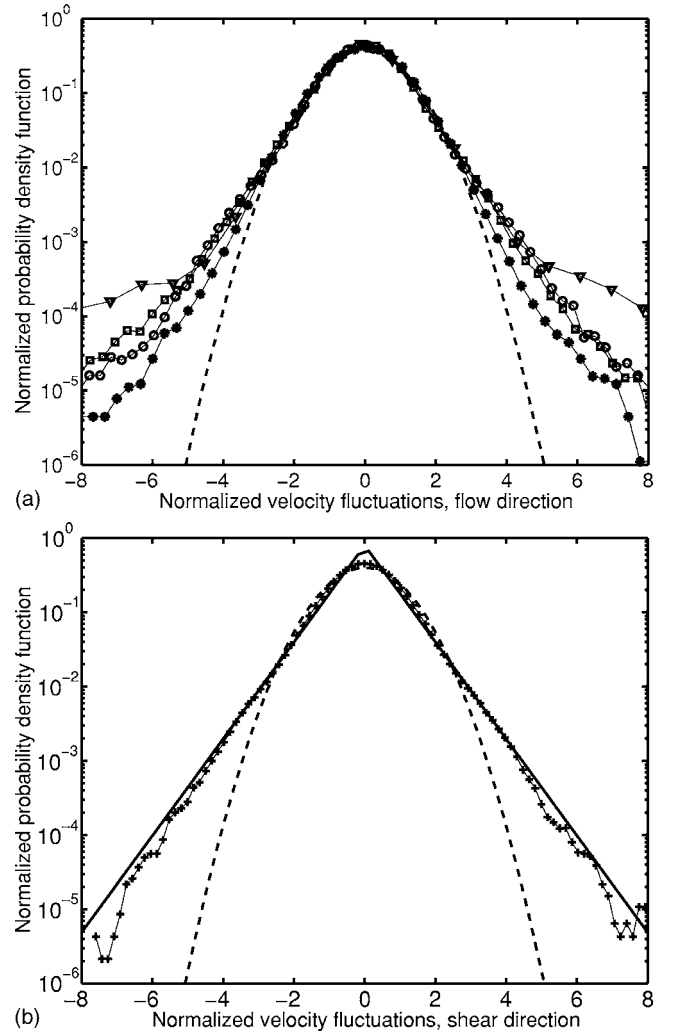


FIG. 7. Normalized PDF of particle velocity fluctuations in the flow direction (symbols), compared to the Gaussian distribution function (dashed line). (a) Triangles:  $\phi=1\%$ ; circles:  $\phi=5\%$ ; squares:  $\phi=10\%$ ; stars:  $\phi=20\%$ . (b) Plus:  $\phi=5\%$ . Solid line; best fit of the PDF by the stretched exponential function  $\text{PDF}(v/s) \approx 2/\sqrt{2\pi} \exp(-1.5|v/s|)$ .

tions are achieved around  $8/G$  nondimensional time units and slightly shorter for more concentrated suspensions.

Finally, the long time uncorrelated fluctuations induce a stochastic transport of the particles in the shear flow in spite of the deterministic and linear nature of creeping flows. It is known that at least three interacting particles are necessary to lead to long time unpredictability in Stokes flow. This overall chaotic motion is generally called shear induced self-diffusion. The transverse diffusion coefficient can be determined in two ways. According to the first method, it is calculated from the integral of the velocity autocorrelation function over a long period of time [Eq. (16)],

$$D_{22} = T_{22} \int_0^{\infty} R_{22}(t) dt. \quad (16)$$

The self-diffusion is made dimensionless by  $Ga^2$ . It is the product of the fluctuation level times the Lagrangian integral time scale (convergence of the time integral is displayed in

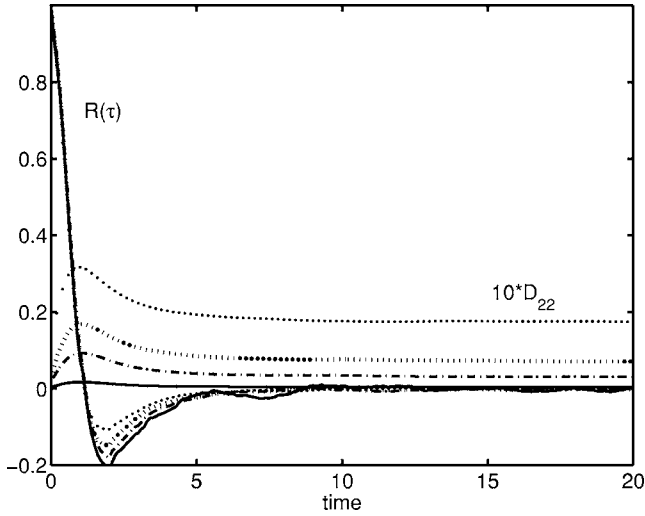


FIG. 8. Normalized Lagrangian autocorrelation function  $R(\tau)$  of the velocity fluctuations and shear induced self-diffusion coefficient  $D_{22}$  calculated by the integration of  $R(\tau)$ : —,  $\phi=1\%$ ; -.-,  $\phi=5\%$ ; ···,  $\phi=10\%$ ; ····,  $\phi=20\%$ .

Fig. 8). It is important to note that we found in our simulations an enhancement of the velocity fluctuations but also an increase of the integral diffusion time with increasing concentration. The second method is based on the long time behavior of the particle mean-square displacement [Eq. (17)]. At short time scale the behavior of the mean-square displacement is not diffusive ( $t^2$  growth rate) and only when the growth becomes linear,  $D_{22}$  can be computed from half of the slope,

$$D_{22} = \frac{1}{2Ga^2} \lim_{t \rightarrow \infty} \frac{d}{dt} \langle (x_2(t) - x_2(0))^2 \rangle. \quad (17)$$

The time evolution of  $\langle (x_2(t) - x_2(0))^2 \rangle / Ga^2$  on a log-log scale (Fig. 9) shows a clear transition from quadratic to linear growth rate after a nondimensional time  $8/G$ . This characteristic time scale is similar to the time required to get

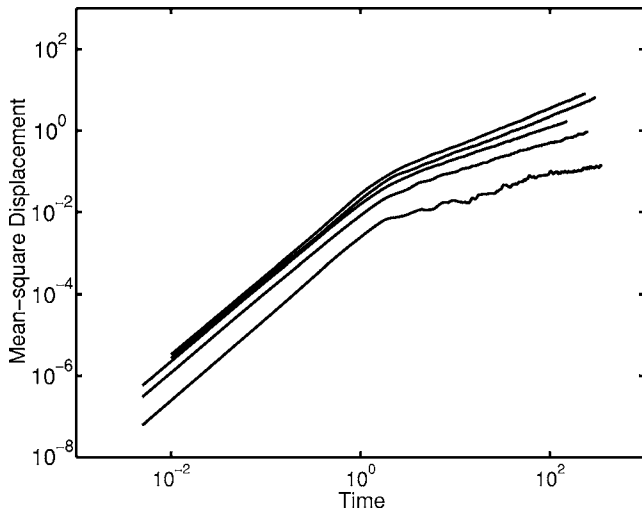


FIG. 9. The temporal evolution of particle mean square displacement  $\langle (x_2(t) - x_2(0))^2 \rangle / Ga^2$ . The curves from bottom to top correspond, respectively, to the concentrations:  $\phi = \{1\%, 5\%, 10\%, 15\%, 20\%\}$ .

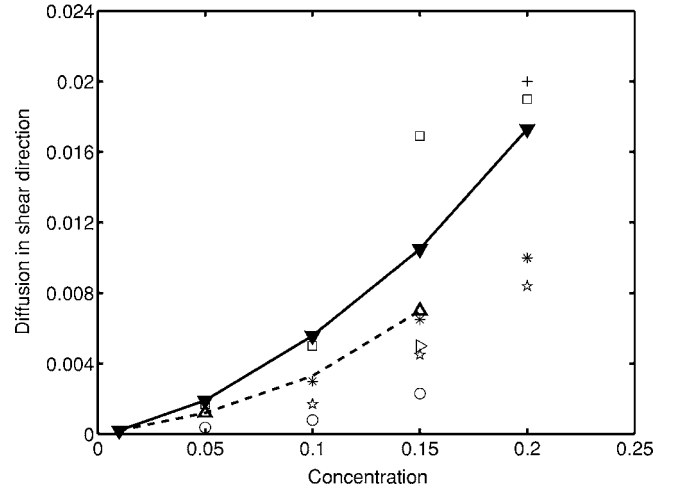


FIG. 10. Shear induced self-diffusion coefficient  $D_{22}$  vs concentration.  $\square$ , experimental work, Leighton and Acrivos (Ref. 33);  $+$ , experimental work, Breedveld *et al.* (Ref. 36);  $*$ , analytic prediction, Acrivos *et al.* (Ref. 61);  $\circ$ , Stokesian dynamics, Drazer *et al.* (Ref. 31);  $\triangleright$ , Stokesian dynamics, Marchioro and Acrivos (Ref. 32);  $\star$ , accelerated Stokesian dynamics, Sierou and Brady (Ref. 37);  $\blacktriangledown$  with solid line: [FCM + barrier repulsion ( $\varepsilon \leq 0.2$ )];  $\Delta$  with dashed line: [FCM + lubrication force ( $\varepsilon \leq 0.2$ ); + barrier repulsion ( $\varepsilon \leq 0.05$ )].

uncorrelated velocity fluctuations (Fig. 8). Such a behavior is characteristic of the diffusion regime and the self-diffusion coefficient may be obtained by half the slope of the linear growth rate. At low concentration, the suspension particles need more time to reach the diffusive behavior. Indeed, the diffusion occurs after each particle encountered multiple interactions with other particles. The time between two consecutive interactions scales with  $\phi^{-1}$  and decreases with increasing concentration. We can notice that both ways of determining the self-diffusion coefficient lead to the conclusion that long time sequences are necessary to achieve a diffusive-like behavior of the suspension. Sierou and Brady<sup>37</sup> claimed that most experiments were flawed due to this limitation.

The self-diffusion coefficient is strongly dependent on the volume fraction of the suspension (Fig. 10). The results we obtained with the FCM are in the range of the former studies. Our simulations stand within the scattered results achieved by theoretical prediction, experimental measurements, and numerical simulations. Indeed, the data in the literature are scattered due to experimental limitations (short time used by Breedveld *et al.*<sup>34</sup> for the diffusion calculation), simulation limitations (discussed in Ref. 37) or theoretical assumptions (Ref. 60). If the diffusion process was controlled by the finite drift induced by the nonhydrodynamic repulsive force, the transverse self-diffusion coefficient would have scaled linearly with the concentration. In an extremely dilute regime, we should recover this linear scaling but statistics are much longer to converge as particle encounters become very rare. Thus, we have tested the effect of the repulsion barrier by varying the amplitude of the force scale at a constant concentration of the suspension. We obtained a scattering of less than 30% for large variations of the repulsion force. Compared to former numerical studies, the self-diffusion coefficient computed with the FCM is slightly

overestimated which is essentially related to the inaccurate representation of the viscous local effects when the lubrication model is not used. In Sec. II C we have checked the effect of the lubrication forces on the relative trajectories of an interacting pair (see comments of Fig. 4). Then, we performed new simulations to achieve the statistical behavior of the suspension ( $\phi=5\%$  and  $\phi=15\%$ ). When improving the local hydrodynamic interactions with the lubrication forces, the new results showed that the simulations with the simple repulsion barrier were not misleading. Translational velocity fluctuations and pdf were correctly evaluated (10% average underestimation). Actually, this can be easily understood. The repulsion force has been calibrated to prevent overlapping and then gives correct prediction of perturbation velocity of interacting particle pairs. The determination of the shear-induced coefficients is more critical because they depend on multibody interactions but also on the finite drift of the particles across streamlines at each particle encounter. When using the lubrication forces, we got a reduction of 35% of the self-diffusion coefficients in the shear and spanwise directions. The agreement with the recent simulations of Sierou and Brady<sup>37</sup> is fairly good.

We also evaluated the self-diffusion coefficient in the spanwise direction  $D_{33}$  following the same ways. We found that it behaves similarly as  $D_{22}$  when the concentration increases with the same qualitative agreement with the previous works. However, we found that the self-diffusion tensor at a fixed solid fraction is anisotropic, i.e.,  $D_{22}/D_{33} \sim 1.5$ , in agreement with the other experimental and numerical investigations (Refs. 31 and 35).

## B. Bidisperse suspensions

Based on the description of the dynamics of monodisperse suspension, it is of major interest to investigate bidisperse suspensions undergoing shear as most of the practical applications are concerned with highly polydisperse particle distributions. Statistical quantities may be scaled by an average particle diameter with the assumption that the qualitative behavior does not depend on the size. The analysis of the results on bidisperse suspensions is more complicated since it depends simultaneously on many nondimensional parameters (see the Introduction). Varying all the parameters requires an enormous amount of independent simulations. To the best of our knowledge, only two works (Refs. 38 and 39) have proposed a detailed statistical study of polydisperse suspensions under shear, but these are limited to simulations in two dimensions and rather high concentration.

In all the suspensions that we have considered in this part, the density ratio  $\gamma=1$  and we neglect the effect of buoyancy. The suspension is homogeneous as particles are initially randomly seeded regardless of their size. We carefully checked that initial positions and trajectories were not overlapping. At low to moderate concentration, homogeneity is preserved because particle interlocking is not occurring. This is completely different from the dynamics observed by Chang and Powell<sup>39</sup> at concentrations close to packing. They found that the formation of clusters of the particle is the major point that drives the macroscopic behavior of the sus-

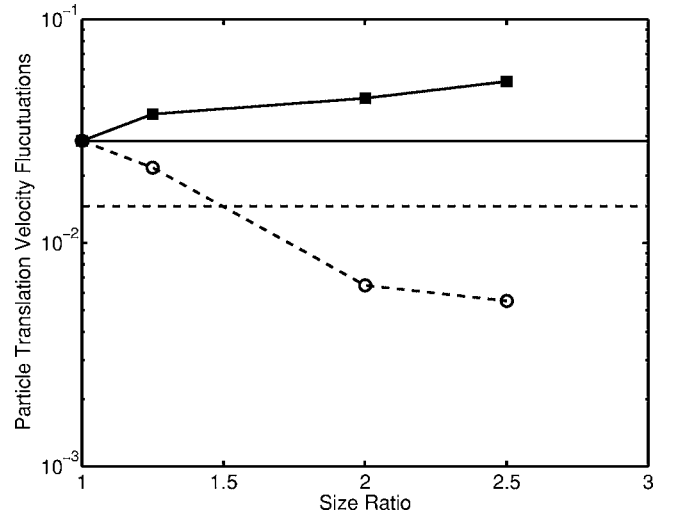


FIG. 11. Velocity fluctuations in the shear direction  $T_{22}$  vs the size ratio  $\lambda$  ( $\phi=10\%$ ;  $\phi_2/\phi_1=1$ ). Filled squares with solid line: small particles; empty circles with dashed line: large particles. Horizontal lines: fluctuation level for a monodisperse suspension (FCM) (solid line  $\phi=10\%$ , dashed line  $\phi=5\%$ ).

pension. We looked at the suspension microstructure through the pair probability density functions ( $g_{11}$ ,  $g_{12}$ , and  $g_{22}$ ) and we have observed that particle pairs of different sizes are occurring.

First, we fixed a constant total volume fraction of the suspension  $\phi=\phi_2+\phi_1=10\%$  and we studied the effect of varying either the size ratio  $\lambda$  for a given concentration ratio  $\phi_2/\phi_1$  (index 2 stands for the large particles) or we varied the concentration ratio for a given size ratio.

Figure 11 shows the evolution of the translational velocity fluctuations for  $\phi_2/\phi_1=1$ . The fluctuation levels of both species have been scaled with respect to their respective size. This dimensionless representation eases the analysis as the comparison with a monodisperse equivalent configuration is straightforward. On the same plot, we compared the fluctuation levels to the case of a monodisperse suspension having either a volume fraction of 5% or 10%. The behavior of the fluctuations is qualitatively different for the two species. As the size ratio increases, the velocity fluctuations of the small particles is enhanced compared to a monodisperse case at the same total concentration. For instance, when  $\lambda=2.5$ , the velocity fluctuations of the small particles is almost twice the monodisperse case. The large particles experience an opposite trend as the presence of small particles seems to hinder fluctuations of this specie. Velocity fluctuations of the large particles are eventually lower than if they were alone in the suspension (monodisperse  $\phi=5\%$ ). The same trend is obtained for fluctuations in other directions, as well as for the transverse shear induced self-diffusion coefficient (Fig. 12).

Then, for a given size ratio ( $\lambda=2$ ), Figs. 13 and 14 quantify the impact of varying the concentration ratio ( $\phi_2/\phi_1$ ) on the statistical quantities. The fluctuations as well as the diffusion coefficients for both species increase while the amount of large particles increases ( $\phi_2/\phi_1=1/9$  corresponds to 10% of large particles and  $\phi_2/\phi_1=9$  corresponds to 90%). We compared this with the reference case of a 10% total

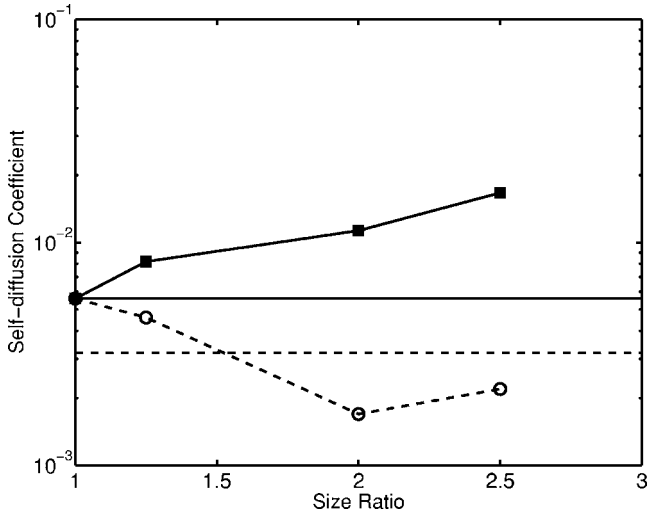


FIG. 12. Shear induced self-diffusion coefficient in the shear direction  $D_{22}$  vs the size ratio  $\lambda$  ( $\phi=10\%$ ;  $\phi_2/\phi_1=1$ ). Filled squares with solid line: small particles; empty circles with dashed line: large particles. Horizontal lines: diffusion coefficient for a monodisperse suspension (FCM) (solid line  $\phi=10\%$ ; dashed line  $\phi=5\%$ ).

concentration for a monodisperse suspension. For low (respectively, large) concentration ratio, the fluctuation level and the self-diffusion coefficient are approaching their monodisperse value for the small (respectively, large) particles. The fluctuations of small particles are strongly enhanced by the presence of the large particles (velocity fluctuations are almost doubled when the concentration ratio  $\phi_2/\phi_1$  increases from 1/9 to 9). Chang and Powell<sup>39</sup> found a similar behavior even when the suspension is relatively concentrated (total equivalent volume fraction of 35%). Because of the interlocking phenomenon in dense suspension, the authors observed a slight minimum in the evolution of the self-diffusion coefficient with the concentration ratio when the amount of small spheres becomes dominant. Furthermore, we plotted in Fig. 14 the self-diffusion coefficients for small

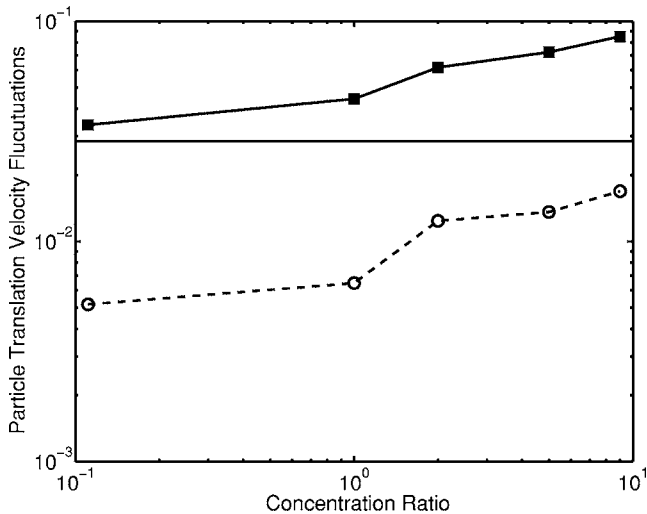


FIG. 13. Velocity fluctuations in the shear direction  $T_{22}$  vs the concentration ratio  $\phi_2/\phi_1$  ( $\phi=10\%$ ;  $\lambda=2$ ). Filled squares with solid line: small particles; empty circles with dashed line: large particles. Horizontal solid line: fluctuation level for a monodisperse suspension  $\phi=10\%$  (FCM).

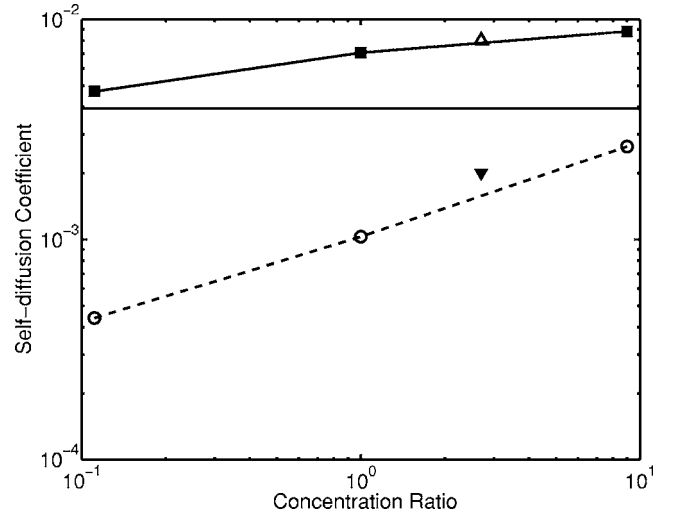


FIG. 14. Shear induced self-diffusion coefficient in the spanwise direction  $D_{33}$  vs the concentration ratio  $\phi_2/\phi_1$  ( $\phi=10\%$ ;  $\lambda=2$ ). Filled squares with solid line: small particles; empty circles with dashed line: large particles. Triangles: Chang and Powell (Ref. 39);  $\triangle$ : small particles;  $\nabla$ : large particles. Horizontal solid line: diffusion coefficient for monodisperse suspension  $\phi=10\%$  (FCM).

and large particles obtained by Chang and Powell,<sup>39</sup> choosing the suspension composition as close as possible to our simulation conditions (i.e., two-dimensional bidisperse suspension with a 12% total area fraction which is equivalent to our three-dimensional suspension with a total volume fraction of 8%). We divided their results by 1.5 (anisotropy coefficient) to obtain the equivalent self-diffusion coefficients in the spanwise direction in order to compare with our results. Then we compared the fluctuations (translational velocity and rotation rate) of the two species in Fig. 15. We noticed that the ratio of large to small particle fluctuations is only slightly varying with the concentration ratio. The fluctuations of the large particles are nearly half the fluctuations of the small ones. The analysis of the pair probability density

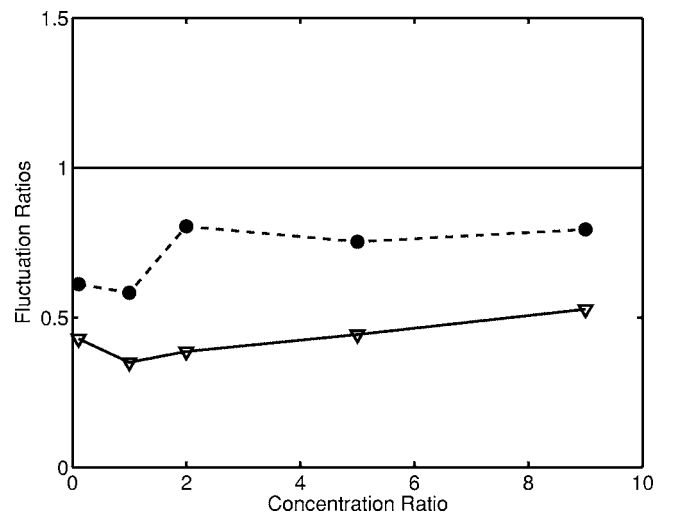


FIG. 15. Ratios of the translational and rotational fluctuations of the large particles over the small ones vs the concentration ratio  $\phi_2/\phi_1$  ( $\phi=10\%$ ;  $\lambda=2$ ). Empty triangles with solid line:  $w_{33}$ . Filled circles with dashed line:  $T_{22}$ .

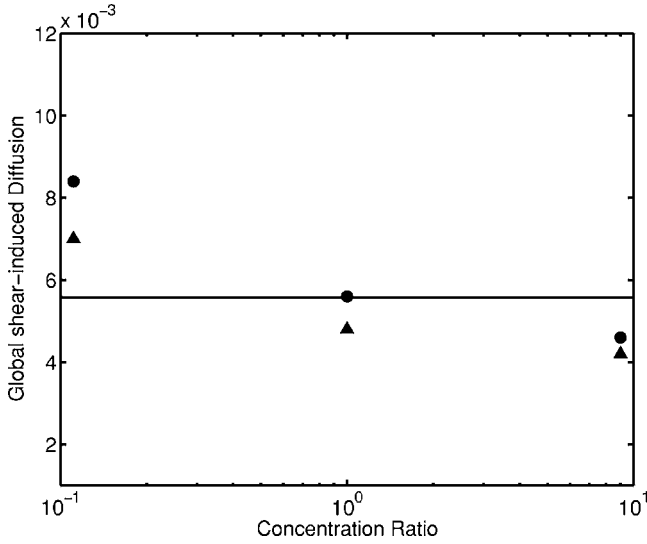


FIG. 16. Global shear induced diffusion  $D_g$  in the shear direction vs the concentration ratio  $\phi_2/\phi_1$  ( $\phi=10\%$ ). Horizontal solid line:  $D_{22}$  in a monodisperse suspension  $\phi=10\%$ . Filled circles:  $\lambda=2.5$ . Filled triangles:  $\lambda=2$ .

functions reveals that even a small amount of large particles ( $\phi_2/\phi_1=1/9$ ) could enhance intense fluctuations of the small particles leading to prominent exponential tails. The opposite trend was observed for the large particles. A small amount of small particles ( $\phi_2/\phi_1=9$ ) does not change the Gaussian shape of the pdf for the large particles which was observed at moderately concentrated suspension ( $\phi=10\%$ ).

Instead of examining the distinct statistics of each species, it would also be interesting to quantify the macroscopic behavior of the suspension as a whole. In experiments, it is almost impossible to measure distinctly the characteristics of each species and averages are formed over polydisperse particles. Krishnan and Leighton<sup>62</sup> proposed two definitions of the self-diffusion coefficient averaged in a bidisperse suspension. The “global” shear induced diffusion coefficient  $D_g$  of all the particles is obtained from the mean-square displacement of all the particles (regardless of their size) and it is scaled with the particle average radius  $\langle a \rangle$  [Eq. (18)],

$$\langle a \rangle = \frac{a_1 \phi_1 + a_2 \phi_2}{\phi_1 + \phi_2}. \quad (18)$$

Figure 16 shows that, for a given size ratio and total concentration ( $\phi=10\%$ ) of the suspension, the global diffusion coefficient is larger than the monodisperse case at low concentration ratio. Thus, the reduction of the diffusion coefficient is nearly 50% when  $\phi_2/\phi_1$  increases from 1/9 to 9. This suggests that the presence of a small amount of large particles enhances the diffusion in the whole suspension. But when large particles are dominant, the trend is opposite as velocity fluctuations and diffusive phenomenon are reduced. The data can be plotted versus the size ratio for a constant  $\phi_2/\phi_1=1$ . In Fig. 17, the relative variation of the global diffusion coefficient is only 18%. We concluded that  $D_g$  is strongly dependent on the concentration ratio but does not change much with size ratio. It does not seem appropriate to use it at a unique parameter characterizing a polydisperse suspension. The other “mean” diffusion coefficient proposed

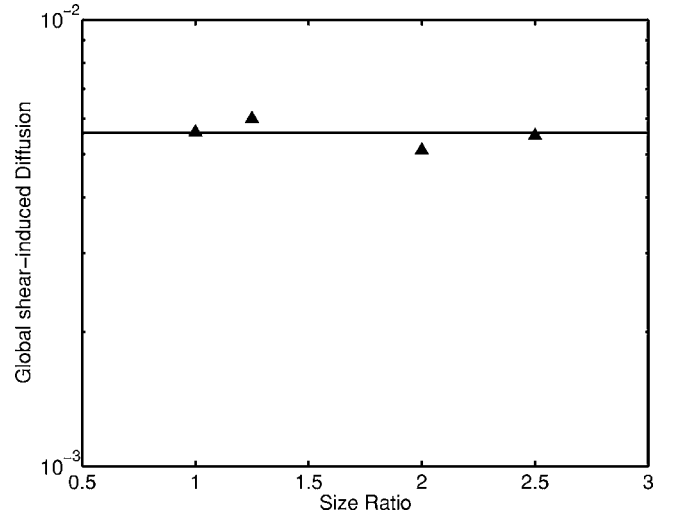


FIG. 17. Global shear induced diffusion  $D_g$  in the shear direction vs the size ratio  $\lambda$  ( $\phi_2/\phi_1=1$ ;  $\phi=10\%$ ). Horizontal solid line:  $D_{22}$  in a monodisperse suspension  $\phi=10\%$ .

by Krishnan and Leighton<sup>62</sup> is defined in Eq. (19),

$$\langle D \rangle = \frac{D_g \langle a \rangle^2}{\frac{\phi_1}{\phi_1 + \phi_2} D_1(\phi) a_1^2 + \frac{\phi_2}{\phi_1 + \phi_2} D_2(\phi) a_2^2}. \quad (19)$$

The global diffusion coefficient  $D_g(\phi)$  is scaled by a weighted average of the diffusion coefficients [ $D_1(\phi)$  and  $D_2(\phi)$ ] for small and large particles at the same total concentration. In their experiments, they determined, respectively, the diffusion coefficients of the small, the large, and the bidisperse particles. In agreement with their results, we found in Fig. 18 that this mean parameter is not appropriate to collapse the data. Therefore, it has not been possible to resolve the issue of the appropriate average particle radius to use while nondimensionalizing the effective diffusivities.

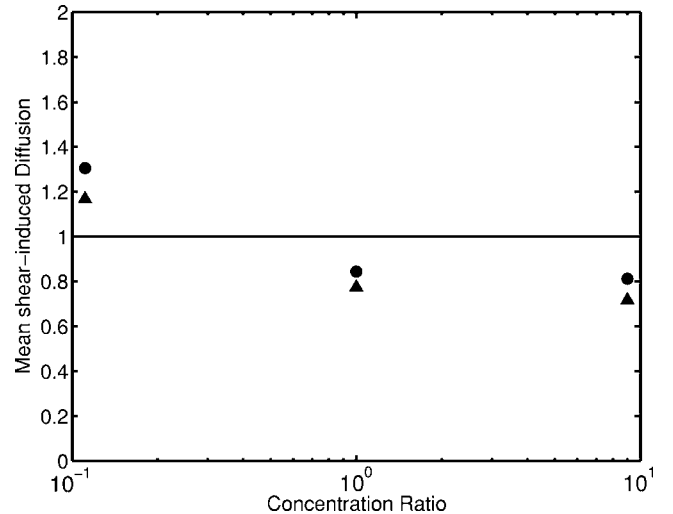


FIG. 18. Mean diffusion coefficient in the shear direction vs the concentration ratio  $\phi_2/\phi_1$  ( $\phi=10\%$ ). Solid line: monodisperse suspension. Filled circles:  $\lambda=2.5$ . Filled triangles:  $\lambda=2$ .

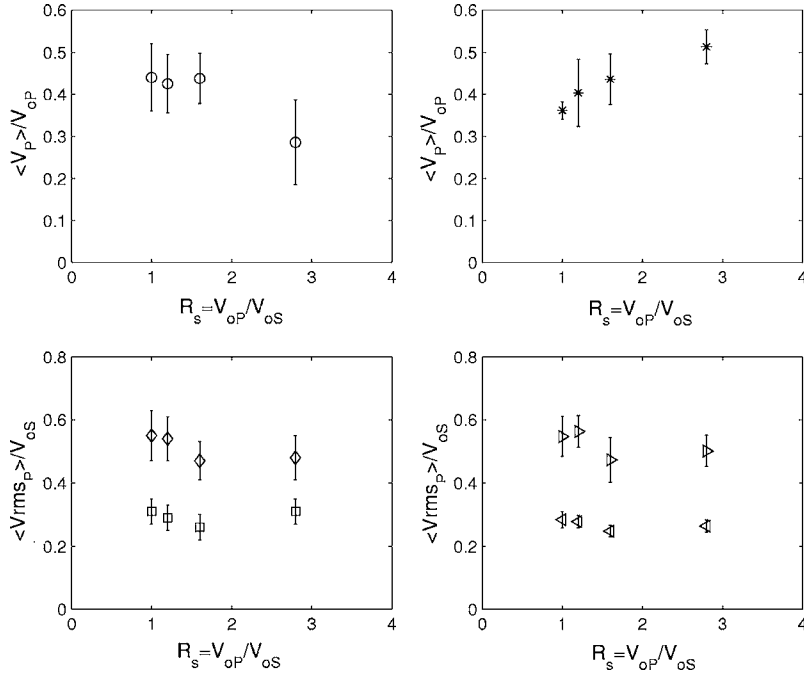


FIG. 19. Settling velocity and fluctuations of a test sphere in a homogeneous suspension. Left column: Experiments of Nicolai *et al.* (Ref. 66). Right column: Numerical simulations with FCM. Top row: mean vertical velocity. Bottom row: vertical fluctuations (diamonds and right triangles); horizontal fluctuations (squares and left triangles).

## IV. BIDISPERSE SETTLING SUSPENSIONS

Precise experimental results on the behavior of polydisperse suspension are extremely difficult because it is almost impossible to separate the contribution of each species in the bulk. Experimental data are often extracted from the settling velocity of the shock fronts separating the fixed sediment, the mixture of the two species, a monodisperse suspension and the supernatant clear fluid. Acoustic techniques (Ref. 63) or light attenuation measurements provide time dependent profiles of concentration that lead to the determination of the settling velocity. Evaluating the bulk velocities from the front motions suffers severe shortcomings if corrections are not included at moderate to high concentration (Ref. 63). Simulations of homogeneous suspensions are then desired to build composite hindrance functions based on size ratio and concentration ratio. A recent paper (Ref. 64) investigated the drag force on fixed arrays of bidisperse spheres. They proposed new improvements of empirical correlations even valid at a large diameter ratio.

### A. Sedimentation of a test particle

The simplest configuration of bidisperse suspension is related to the settling motion of a single test particle through a uniform homogeneous suspension of monodisperse particles. The test particle has physical properties (size and density) different from the other beads of the suspension. This configuration is similar to the “falling ball viscometer” where nonbuoyant particles hinder the settling of a test particle (Ref. 65). In addition to be an instructive test case of the dynamics in a simple bidisperse system, important statistic quantities may be evaluated to feed macroscopic models. A detailed experimental study (Ref. 66) of the evolution of the mean settling velocity and the fluctuation level of the test particle provides a valuable framework to check the response of our numerical model.

The surrounding homogeneous concentration (20%) is kept constant throughout all the simulations. Only the physical properties of the test sphere ( $a_p$  and  $\Delta\rho_p$ ) are varied according to the experimental configurations. The size ratio  $\lambda = a_p/a_s$  varies from 1 to 1.6 and the ratio of reduced densities  $\gamma = \Delta\rho_p/\Delta\rho_s$  is constant and equal to 1. The subscript  $P$  is associated with the test particle, and  $S$  to the particles of the suspension. For a suspension settling under gravity, a useful combination of these parameters defines the ratio of the settling velocities:  $R_s = V_{oP}/V_{oS} = \gamma\lambda^2$  ( $V_o$  being the Stokes velocity of a single particle in an unbounded quiescent fluid). Averages are formed over long time sequences (more than 400 Stokes time) and different random initial seeding. Figure 19 shows that the agreement is good between the experiments and the simulations. The largest discrepancy occurs with the configuration  $R_s = 2.8$ . Nicolai *et al.*<sup>66</sup> have investigated the range  $R_s = 1$  to  $R_s = 13$  and the experimental point associated with  $R_s = 2.8$  is clearly below the mean trend of their own results. The experimental data are rather scattered around  $\langle V_p \rangle / V_{oP} = 0.42$ . They interpreted this result as a constant effective viscosity of the suspension while particle volume fraction was kept constant at 20%. The evolution of the level of vertical and horizontal fluctuations is in very good agreement with the experimental data. The error bars have to be carefully interpreted because in simulations they are related to standard deviation of the mean value. The velocity fluctuations generally have a Gaussian distribution as it was observed in the experiments and the long-time motion of the test sphere is diffusive due to many body interactions.

Based on the numerical trajectories, the Lagrangian velocity autocorrelation functions [Fig. 20(a)] indicate that fluctuating velocities are correlated on time scales of the order of 10–20 Stokes times ( $a_s/V_{oS}$ ). In agreement with the experiments of Nicolai *et al.*,<sup>66</sup> we found in our simulations that the test particle settles through the suspension with a



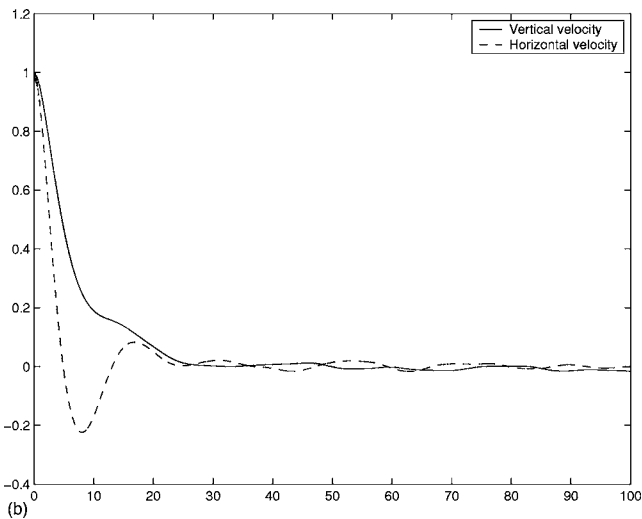
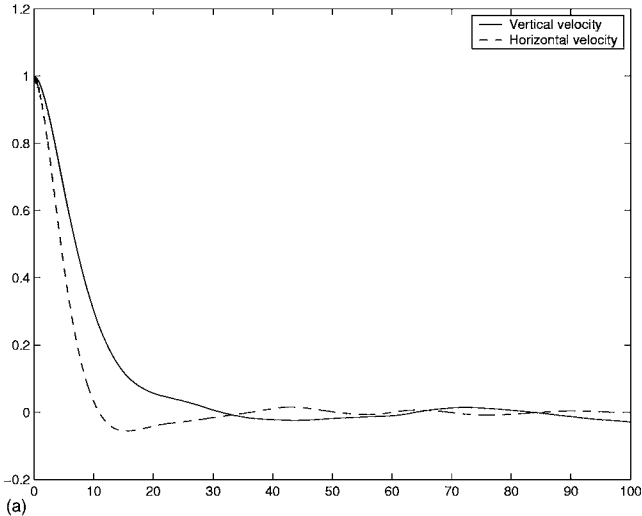


FIG. 20. Normalized Lagrangian velocity autocorrelation function of a single test sphere in a suspension (FCM simulations). Solid line: vertical velocity; dashed line: horizontal velocity. (a)  $R_S=1.2$ ; (b)  $R_S=2.8$ .

larger velocity when the autocorrelation function of the horizontal velocity has a negative region [Fig. 20(b)]. In the simulations, the behavior of the vertical velocity autocorrelation is rather unchanged when the transition occurs which agrees with the experimental observations (Ref. 66). The negative minimum is located around the dimensionless time  $V_{ost}/a=10$ . The experimental value obtained for the transition regime is around  $R_S=5$  and the dimensionless time around 25. The global trend is a decrease of this time scale with  $R_S$  increasing. A simple interpretation of this transition is related to the modification of the trajectory pattern. When the Lagrangian autocorrelation function exhibits a negative region (the function becomes negative and goes through a minimum before approaching zero from below), a zig-zag motion of the test sphere induces a reduction of the correlation time of the trajectory (anticorrelated velocity occurs on a finite time scale). The self-diffusion coefficient of the test sphere is strongly reduced while it is able to push the other particles apart. This scenario has been confirmed by analysis of animated movies of the simultaneous motions of the test sphere and the suspension particles.

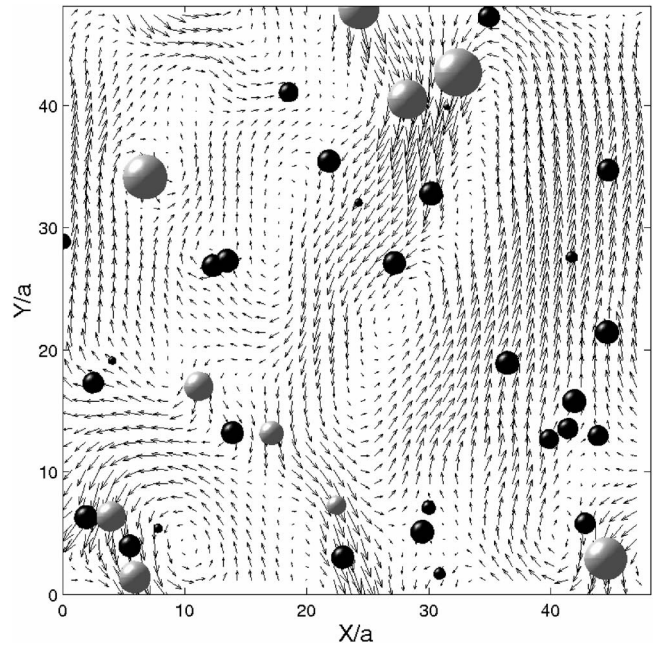


FIG. 21. Bidisperse suspension, ( $\phi=6\%$ ) vertical snapshot (black: small particles; gray: large particles) ( $\phi_1=3\%$  and  $\phi_2=3\%$ ). Size ratio  $\lambda=2$  and density ratio  $\gamma=1$ .

## B. Stable configurations of bidisperse suspensions

As it was observed in monodisperse suspensions (Ref. 67), the flow in a bidisperse suspension is composed of large-scale swirls that tend to collect the particle in clusters (Fig. 21). Long range interactions (slowly decaying like  $1/r$ ) induce multibody hydrodynamic interactions. It has been pointed out that collective motion of nearby particles enhance the local settling velocity while isolated beads experience the back fluid flow leading presumably to high level of fluctuation levels. The presence of two species of different size may also modify the microstructure and influence the relative fluctuations of each species (Ref. 26) but investigations on this topic are almost nonexistent.

In a theoretical analysis of the very dilute regime, Batchelor and Wen<sup>21</sup> proposed linear relations between the mean settling velocities and the concentrations assuming that the suspension is homogenous and that statistics are based on pairwise interactions. The determination of the numerical coefficients is based on the assumption of very dilute systems and perfect random distribution of the particles. The agreement with this theoretical relation has been extensively validated by experiments in the very dilute regime (Refs. 22 and 24). We performed simulations with two different size ratios ( $\lambda=2$  and  $\lambda=3$ ). The average settling rate of both species [Figs. 22(a) and 22(b)] accurately agrees with the prediction of Batchelor and Wen.<sup>21</sup> When the total concentration of the suspension is above 6%, the simulations deviate significantly from the theoretical predictions. Davis and Geol<sup>25</sup> modified these relations to extend their validity to moderately concentrated suspensions. This elegant empirical relation is based on the coefficients derived by Batchelor and Wen<sup>21</sup> and does not require any fitting parameters. It is clear that the smooth transition from dilute to moderately concentrated regimes oc-

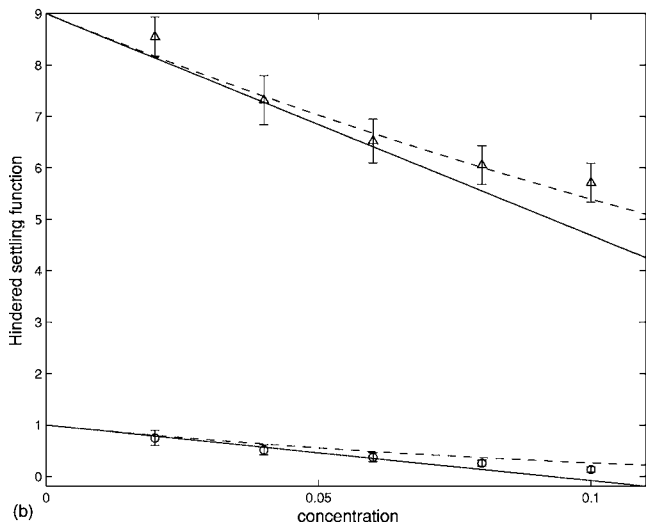
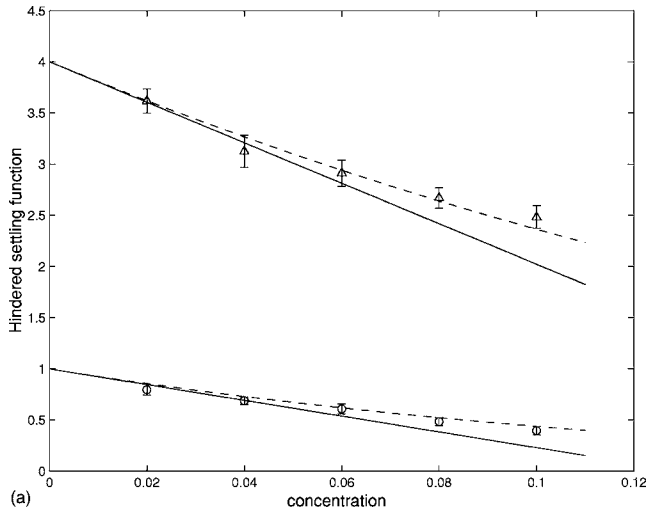


FIG. 22. Mean settling velocity vs total concentration. Solid line: Batchelor and Wen (Ref. 21). Dashed line: Davis and Gecol (Ref. 25). Circles (small particles) and triangles (large particles): FCM numerical simulations ( $\phi_1 = \phi_2 = \phi/2$ ). (a)  $\lambda=2$  and  $\gamma=1$ ; (b)  $\lambda=3$  and  $\gamma=1$ .

curs around 5% and is correctly reproduced by our numerical model. Our simulations agree very well with the two sets of approximation.

We investigated the role of the width of the numerical domain on the evolution of the statistics (Fig. 23) for fixed concentration and size ratios. The mean velocity does not depend on the size of the simulation domain. On the contrary, the level of fluctuations is strongly related to the width of the domain (Ref. 7) and increases with the size of the box. This response of the flow is classic for a purely homogeneous suspension with periodic boundary conditions (Refs. 16 and 68). A scaling of velocity fluctuation levels was proposed by Peysson and Guazzelli.<sup>26</sup> They proposed to use two different length scales to collapse their data and suggested that the microstructure may be affected by the presence of large and small particles. Our simulations seem to indicate that a bidisperse purely homogeneous suspension is subject to a divergent evolution of the fluctuation levels but further studies are still required. When periodic boundary conditions are treated as solid impermeable walls, Nguyen and Ladd<sup>19</sup> showed that density fluctuations are finite at all scales leading a domain size independent behavior of the velocity fluctuation levels even with a small amount of polydispersity. In this case, stratification due to differential settling is a possible mechanism for screening hydrodynamic long range interactions.

While keeping the size ratio  $\lambda$  constant, a “bidisperse” suspension can be achieved with the same particle radius but various reduced densities. In Figs. 24(a) and 24(b), we compare the FCM results with former theoretical and numerical predictions. The concentration of the first species is kept constant ( $\phi_1=0.02$ ). When the two species are sedimenting along the direction of gravity ( $\gamma=2$ ) both settling rates decrease with the total concentration. This is in qualitative agreement with former theoretical predictions of Batchelor and Wen,<sup>21</sup> empirical relation of Davis and Gecol<sup>25</sup> or numerical simulations of Revay and Higdon.<sup>27</sup> When buoyant and heavy particles are mixed,  $\gamma$  is negative. In the particular

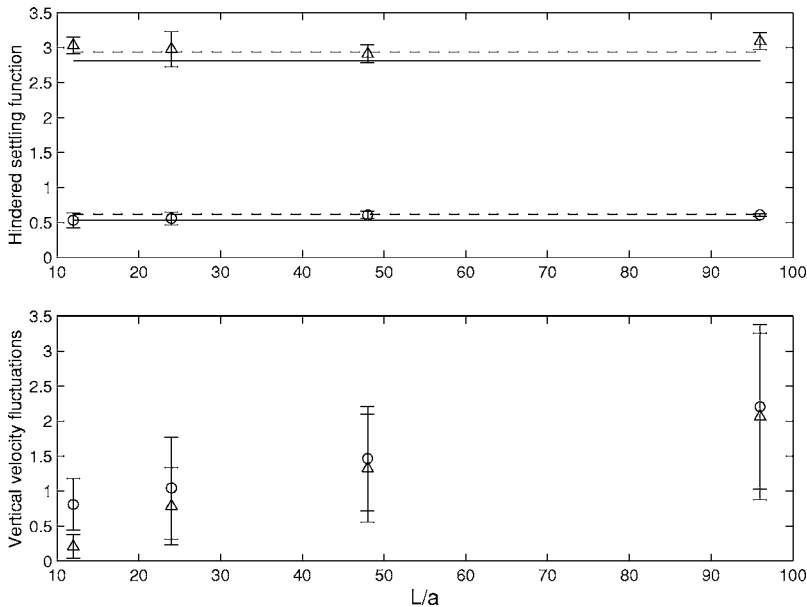


FIG. 23. Variation of the statistics with the width of the domain ( $c=6\%$ ). Solid line: Batchelor and Wen (Ref. 21). Dashed line: Davis and Gecol (Ref. 25). Circles and triangles: numerical simulations ( $\phi_1 = \phi_2 = \phi/2$ ,  $\lambda=2$  and  $\gamma=1$ ). Error bars characterize the standard deviation of the mean value.

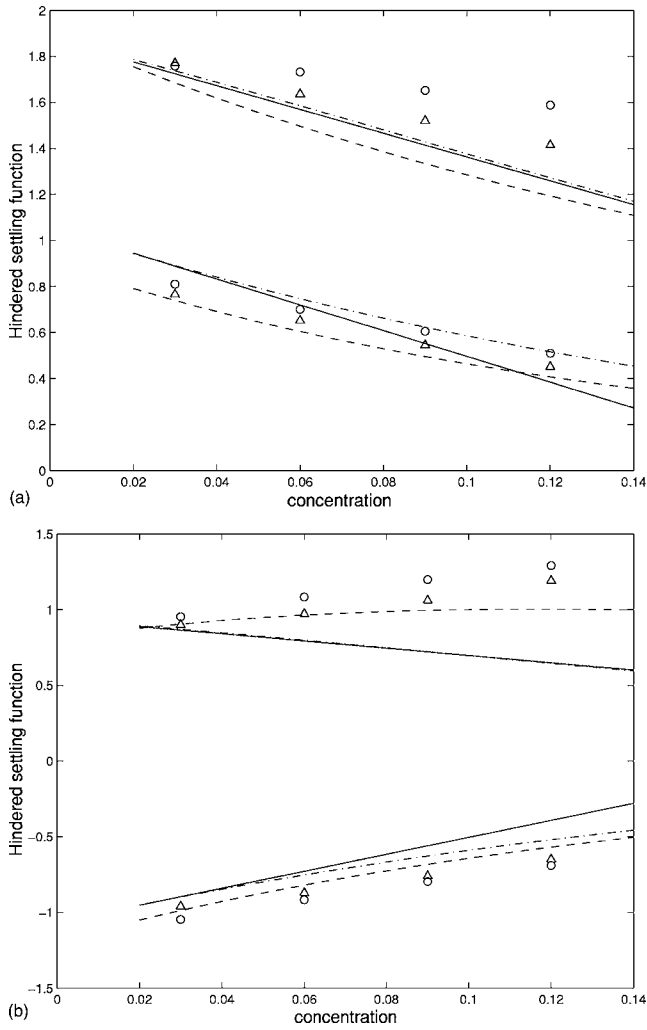


FIG. 24. Mean settling velocity of a monodisperse suspension ( $\lambda=1$ ) with different density ratios. Total concentration  $\phi=0.02+\phi_2$ . (a) ( $\lambda=1$ ;  $\gamma=2$ ). (b) ( $\lambda=1$ ;  $\gamma=-1$ ). Solid line: Batchelor and Wen (Ref. 21). Dotted-dashed line: Davis and Gecol (Ref. 25). Dashed line: Revay and Higdon (Ref. 27). Triangles: static FCM simulations. Circles: dynamic FCM simulations.

case of  $\gamma=-1$ , the settling and rising velocities of individual particles have the same magnitude but opposite signs. We kept constant the concentration of the rising species and increase gradually the total concentration. As the concentration of the settling phase is increased, the buoyant particles experience the net upward flux of fluid. Therefore the average velocity of the light species increases continuously with  $\phi$  [Fig. 24(b)]. Such an enhanced creaming velocity is only reproduced by the numerical model proposed by Revay and Higdon<sup>27</sup> whereas the prediction of Batchelor and Wen<sup>21</sup> has the wrong trend. We observed that the dynamic simulations provide a larger rising velocity than the average based on random static interactions. The cause of such an increase is probably related to a preferential migration of the light particles in upstream currents. Simulations of Revay and Higdon<sup>27</sup> were performed with a static procedure (ensemble averaging on different random seeding) and their results are surely underestimating the dynamic behavior. We can see that the agreement is very good with our present static simulations.

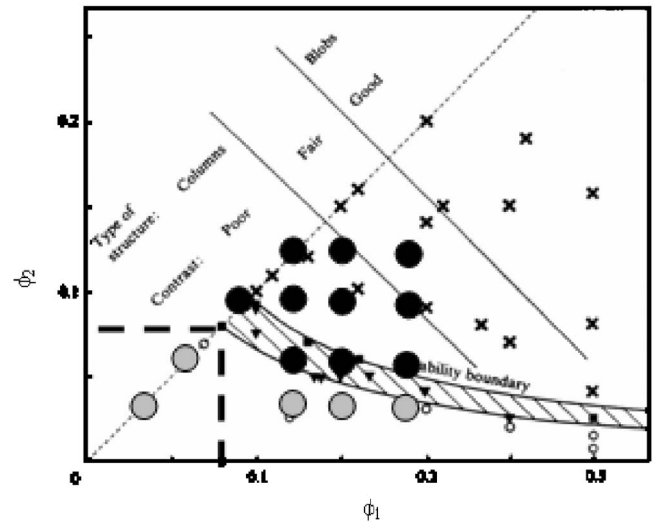


FIG. 25. Stability diagram from the experiments of Batchelor and Van Rensburg (Ref. 43) with buoyant and heavy particles of equal size ( $\lambda=1$ ;  $\gamma=-1$ ). The plot is symmetric when interchanging  $\phi_1$  and  $\phi_2$ . Large circles: FCM simulations (gray: stable, black: unstable).

### C. Segregation instability

For a suspension composed of heavy and light particles ( $\lambda=1$ ,  $\gamma=-1$ ), when the volume fraction of the two species is increased beyond a critical concentration (around 15% total), an instability of the suspension sets in. The particles tend to segregate and form vertical streams composed of only one type of particle. This phenomenon has been observed experimentally (Refs. 42 and 43) and some stability analyses (Refs. 43, 69, and 70) are available but the fundamental origin of this phenomenon is still lacking.

Particles are initially seeded at random positions in the simulation domain regardless of their density. Then, particles freely evolve under mutual hydrodynamic interactions. Below the critical value of 15%, the suspension remains stable (perfectly mixed). Above the threshold, particles migrate laterally during a transient time and eventually a complete segregation occurs. As periodic boundary conditions are imposed in the simulation, the two vertical streams grow until the box is divided in two distinct regions populated, respectively, with light or heavy particles. During the transient evolution of the suspension, the average velocity of the particles remains nearly constant and suddenly increases as particles of the same species are gathering. The duration of this transient depends on the magnitude of the repulsive barrier we used but the overall dynamics is preserved. The simulated instability threshold is in agreement with the phase diagram of the instability summarizing the experimental works of Weiland *et al.*<sup>42</sup> and Batchelor and Van Rensburg<sup>43</sup> (see Fig. 25). Considering a local density fluctuation of the suspension, the flux of particles can be due to the gradient of concentration that induces migration of particles. As particles are settling and rising in the same fluid flow, they will create local shear layers too, that may be growing and merging. We investigated the pair probability function of each species to elucidate the basic segregation phenomenon. The transition from well mixed to the segregated state is sharp and statistics

were not sufficiently converged to propose a comprehensive scenario of interaction between disturbance amplification and microstructure modification. This point will need further investigations.

## V. CONCLUSION

The aim of the paper was to investigate with the FCM the simulation of homogeneous bidisperse suspensions under two fundamental situations: linear shear flow and sedimentation under gravity. Validation on simple analytic test cases allows a precise evaluation of the accuracy of the model. The far field hydrodynamic interactions are always correctly achieved but when particles are close to contact the lubrication effects are not well reproduced. Such short range interactions can be restored by including lubrication forces as described in Ref. 55. Therefore, we limited our simulations to a maximum concentration of 20%. We have shown that the overall dynamics is in agreement with theories and experiments when the system is moderately concentrated.

The configuration of a monodisperse sheared suspension under Stokes flow has been well documented recently by precise computations using the Stokesian dynamics (Refs. 30, 32, and 37). We computed macroscopic properties like translational and rotational velocity fluctuation tensors and their probability distribution function, Lagrangian velocity autocorrelation function, and shear induced self-diffusion coefficients. Basically, we showed that, when the suspension concentration increases, particle velocity fluctuations are larger, more homogeneous and less correlated. Our numerical results achieved in general a good agreement with previous experimental and numerical works. A repulsion force was used in the simulations to prevent numerical overlapping and it led to an enhancement of the shear induced self-diffusion. The role played by a similar force has been discussed by Da Cunha and Hinch.<sup>58</sup> When the local viscous effects between close interacting particles were properly resolved using the lubrication model (Dance and Maxey<sup>55</sup>), the quantitative agreement of statistical quantities was improved but the overall qualitative behavior of the suspension is similar to the simplified simulations. Although the self-diffusion coefficients are slightly overpredicted by the FCM, they still stand within the range of the available data. The behavior of sheared suspensions is more intricate when two species are mixed. We investigated the macroscopic properties of the suspension by separately varying the size ratio and the respective concentration of each species. For a fixed concentration ratio, we found that an increasing size ratio leads to an enhancement of the fluctuation level of small particles whereas the large particles disperse much less. Then, for a fixed size ratio and total concentration, increasing the relative amount of large particles induces for all particles an enhancement of the fluctuations and particle diffusion.

Investigating the response of a single settling test sphere in a monodisperse suspension is a fundamental issue for the description of the global behavior of a bidisperse suspension. A drastic modification of the horizontal velocity autocorrelation function was observed when the Stokes velocity ratio is above a critical threshold. The test particle tended to settle

with a zig-zag trajectory corresponding to a lower value of the lateral diffusion coefficient.

When two different species are mixed and settle under gravity in a very dilute homogeneous suspension, the theoretical analysis of Batchelor and Wen<sup>21</sup> provides a good prediction of average velocities. In more concentrated media, the empirical relation of Davis and Gecol<sup>25</sup> is more appropriate. Our simulations matched precisely the transition from dilute to moderately concentrated suspension. The particular case of buoyant and heavy particles is a critical configuration because the buoyant species experiences the upward flux of fluid displaced by the sedimenting phase and then the rising velocity increases with the concentration. Above a critical value of the respective concentrations, the particles segregate and two distinct vertical currents develop. This instability is well-known in the literature but no physical scenario has been proposed. Our simulation model was able to reproduce the transient behavior of the segregation process and the phase diagram of stability. To the best of our knowledge, our results are the first Eulero-Lagrangian simulations of the dynamic growth of the segregation instability.

We concluded that the FCM is a good compromise between flexibility and accuracy of hydrodynamic interactions. It was able to reproduce some intricate features like shear-induced diffusion and settling instability. The treatment of bidisperse or more generally polydisperse suspensions is straightforward. It is also possible to include finite inertia of fluid and particles by switching the solution of Stokes equations to Navier-Stokes equations (Ref. 17). The addition of interparticle forces based, for example, on magnetic attraction (Ref. 71) or DLVO theory are easy to implement and open a wide area of investigation on complex suspensions.

## ACKNOWLEDGMENTS

Simulations were performed on local (Calmix) and national French supercomputing centers (IDRIS/CINES). The authors gratefully acknowledge their technical support. The collaboration was funded under a PICS CNRS-USA program. We acknowledge the scientific cooperative structure FERMaT. M.R.M. also acknowledges support from the National Science Foundation under Grant No. CTS-0326702.

<sup>1</sup>G. P. Krishnan, S. Beimfohr, and D. T. Leighton, "Shear-induced radial segregation in bidisperse suspensions," *J. Fluid Mech.* **321**, 371 (1996).

<sup>2</sup>M. O. Toivakka and D. E. Eklund, "Prediction of suspension rheology through particle motion simulation," *Tappi J.* **79**, 211 (1996).

<sup>3</sup>G. K. Batchelor, "Sedimentation in a dilute dispersion of spheres," *J. Fluid Mech.* **52**, 245 (1972).

<sup>4</sup>J. F. Richardson and W. N. Zaki, "Sedimentation and fluidization," *Trans. Inst. Chem. Eng.* **32**, 35 (1954).

<sup>5</sup>R. Buscall, J. W. Goodwin, R. H. Ottewill, and T. F. Tadros, "The settling of particles through Newtonian and non-Newtonian media," *J. Colloid Interface Sci.* **85**, 78 (1982).

<sup>6</sup>R. E. Caflish and J. H. C. Luke, "Variance in the sedimentation speed of a suspension," *Phys. Fluids* **28**, 759 (1985).

<sup>7</sup>E. J. Hinch, "Sedimentation of small particles," in *Disorder and Mixing*, edited by E. Guyon, J.-P. Nadal, and Y. Pomeau (Kluwer Academic, Norwell, 1988), pp. 153–161.

<sup>8</sup>H. Nicolai and E. Guazzelli, "Effect of the vessel size on the hydrodynamic diffusion of sedimenting spheres," *Phys. Fluids* **7**, 3 (1995).

<sup>9</sup>A. J. C. Ladd, "Hydrodynamic screening in sedimenting suspensions of non-Brownian spheres," *Phys. Rev. Lett.* **76**, 1392 (1996).

- <sup>10</sup>M. P. Brenner, "Screening mechanisms in sedimentation," *Phys. Fluids* **11**, 754 (1999).
- <sup>11</sup>D. L. Koch and E. S. G. Shaqfeh, "Screening in sedimenting suspensions," *J. Fluid Mech.* **224**, 275 (1991).
- <sup>12</sup>J. H. C. Luke, "Decay of velocity fluctuations in a stably stratified suspension," *Phys. Fluids* **12**, 1619 (2000).
- <sup>13</sup>S. T. Tee, P. J. Mucha, L. Cipelletti, S. Manley, M. P. Brenner, P. N. Segrè, and D. A. Weitz, "Nonuniversal velocity fluctuations of sedimenting particles," *Phys. Rev. Lett.* **89**, 054501 (2002).
- <sup>14</sup>P. J. Mucha, S. T. Tee, D. A. Weitz, B. I. Shraiman, and M. P. Brenner, "A model for velocity fluctuations in sedimentation," *J. Fluid Mech.* **501**, 71 (2004).
- <sup>15</sup>A. J. C. Ladd, "Dynamical simulations of sedimenting spheres," *Phys. Fluids A* **A5**, 299 (1993).
- <sup>16</sup>A. J. C. Ladd, "Sedimentation of homogeneous suspensions of non-Brownian spheres," *Phys. Fluids* **9**, 491 (1997).
- <sup>17</sup>E. Climent and M. R. Maxey, "Numerical simulations of random suspensions at finite Reynolds numbers," *Int. J. Multiphase Flow* **29**, 579 (2003).
- <sup>18</sup>S. L. Dance and M. R. Maxey, "Density stratification in transient sedimentation," *Phys. Rev. E* **68**, 031403 (2003).
- <sup>19</sup>N. Q. Nguyen and A. J. C. Ladd, "Sedimentation of hard-sphere suspensions at low Reynolds number," *J. Fluid Mech.* **525**, 73 (2005).
- <sup>20</sup>D. Jeffrey and Y. Onishi, "Calculation of the resistance and mobility functions for two unequal spheres in low-Reynolds-number flows," *J. Fluid Mech.* **139**, 261 (1984).
- <sup>21</sup>G. K. Batchelor and C.-S. Wen, "Sedimentation in a dilute polydisperse system of interacting spheres," *J. Fluid Mech.* **124**, 495 (1982).
- <sup>22</sup>R. H. Davis and K. H. Birdsell, "Hindered settling of semidilute monodisperse and polydisperse suspension," *AIChE J.* **34**, 123 (1988).
- <sup>23</sup>D. Bruneau, R. Anthore, F. Feuillebois, X. Auvray, and C. Petipas, "Measurement of the average velocity of sedimentation in a dilute polydisperse suspension of spheres," *J. Fluid Mech.* **221**, 577 (1990).
- <sup>24</sup>M. A. Al-Naafa and M. Sami Selim, "Sedimentation of monodisperse and bidisperse hard-sphere colloidal suspensions," *AIChE J.* **38**, 1618 (1992).
- <sup>25</sup>R. H. Davis and H. Gecol, "Hindered settling function with no empirical parameters for polydisperse suspensions," *AIChE J.* **40**, 570 (1994).
- <sup>26</sup>Y. Peysson and E. Guazzelli, "Velocity fluctuations in a bidisperse sedimenting suspension," *Phys. Fluids* **11**, 1953 (1999).
- <sup>27</sup>J. M. Revay and J. J. L. Higdon, "Numerical simulation of polydisperse sedimentation: Equal sized spheres," *J. Fluid Mech.* **243**, 15 (1992).
- <sup>28</sup>F. R. Da Cunha, G. C. Abade, A. J. Sousa, and E. J. Hinch, "Modeling and direct simulation of velocity fluctuations and particle-velocity correlations in sedimentation," *J. Fluids Eng.* **124**, 957 (2002).
- <sup>29</sup>G. K. Batchelor and J. T. Green, "The hydrodynamic interaction of two small freely-moving spheres in a linear flow field," *J. Fluid Mech.* **56**, 375 (1972).
- <sup>30</sup>G. Drazer, J. Koplik, B. Khusid, and A. Acrivos, "Microstructure and velocity fluctuations in sheared suspensions," *J. Fluid Mech.* **511**, 237 (2004).
- <sup>31</sup>G. Drazer, J. B. Khusid, and A. Acrivos, "Deterministic and stochastic behaviour of non-Brownian spheres in sheared suspensions," *J. Fluid Mech.* **460**, 307 (2002).
- <sup>32</sup>M. Marchioro and A. Acrivos, "Shear-induced particle diffusivities from numerical simulations," *J. Fluid Mech.* **443**, 101 (2001).
- <sup>33</sup>D. Leighton and A. Acrivos, "Measurement of shear-induced self-diffusion in concentrated suspensions of spheres," *J. Fluid Mech.* **177**, 109 (1986).
- <sup>34</sup>V. Breedveld, D. Van den Ende, A. Tripathi, and A. Acrivos, "The measurement of the shear-induced particle and fluid tracer diffusivities by a novel method," *J. Fluid Mech.* **375**, 297 (1998).
- <sup>35</sup>V. Breedveld, D. Van den Ende, M. Bosscher, R. J. J. Jongschaap, and J. Mellema, "Measuring shear-induced self-diffusion in a counter-rotating geometry," *Phys. Rev. E* **63**, 021403 (2001).
- <sup>36</sup>V. Breedveld, D. Van den Ende, M. Bosscher, R. J. J. Jongschaap, and J. Mellema, "Measurement of the full shear-induced self-diffusion tensor of noncolloidal suspensions," *J. Chem. Phys.* **116**, 10529 (2002).
- <sup>37</sup>A. Sierou and J. F. Brady, "Shear-induced self-diffusion in non-colloidal suspensions," *J. Fluid Mech.* **506**, 285 (2004).
- <sup>38</sup>C. Chang and R. Powell, "Dynamic simulation of bimodal suspensions of hydrodynamically interacting spherical particles," *J. Fluid Mech.* **253**, 1 (1993).
- <sup>39</sup>C. Chang and R. Powell, "Self-diffusion of bimodal suspensions of hydrodynamically interacting spherical particles in shearing flow," *J. Fluid Mech.* **281**, 51 (1994).
- <sup>40</sup>A. Shauly, A. Wachs, and A. Nir, "Shear-induced particle resuspension in settling polydisperse concentrated suspension," *Int. J. Multiphase Flow* **26**, 1 (2000).
- <sup>41</sup>A. Shauly, A. Wachs, and A. Nir, "Shear-induced particle migration in a polydisperse concentrated suspension," *J. Rheol.* **42**, 1329 (1998).
- <sup>42</sup>R. H. Weiland, Y. P. Fessas, and B. V. Ramarao, "On instabilities arising during sedimentation of two-component mixtures of solids," *J. Fluid Mech.* **142**, 383 (1984).
- <sup>43</sup>G. K. Batchelor and R. W. J. Van Rensburg, "Structure formation in bidisperse sedimentation," *J. Fluid Mech.* **166**, 379 (1986).
- <sup>44</sup>J. F. Brady and G. Bossis, "Stokesian dynamics," *J. Fluid Mech.* **20**, 111 (1988).
- <sup>45</sup>L. Durlofsky, J. F. Brady, and G. Bossis, "Dynamic simulation of hydrodynamically interacting particles," *J. Fluid Mech.* **180**, 21 (1987).
- <sup>46</sup>A. Sierou and J. F. Brady, "Accelerated Stokesian dynamics simulations," *J. Fluid Mech.* **448**, 115 (2001).
- <sup>47</sup>N. A. Patankar, P. Singh, D. D. Joseph, R. Glowinski, and T.-W. Pan, "A new formulation of the distributed Lagrange multiplier/fictitious domain method for particulate flows," *Int. J. Multiphase Flow* **26**, 1509 (2000).
- <sup>48</sup>A. Esmaeeli and G. Tryggvason, "Direct numerical simulations of bubbly flows Part I-II," *J. Fluid Mech.* **377**, 313 (1999).
- <sup>49</sup>M. R. Maxey and B. K. Patel, "Localized force representations for particles sedimenting in Stokes flows," *Int. J. Multiphase Flow* **27**, 1603 (2001).
- <sup>50</sup>S. Lomholt and M. R. Maxey, "Force-coupling method for particulate two-phase flow Stokes flow," *J. Comput. Phys.* **184**, 381 (2003).
- <sup>51</sup>S. Lomholt, B. Stenum, and M. R. Maxey, "Experimental verification of the force coupling method for particulate flows," *Int. J. Multiphase Flow* **28**, 225 (2002).
- <sup>52</sup>H. Nicolai, B. Herzhaft, E. J. Hinch, L. Oger, and E. Guazzelli, "Particle velocity fluctuations and hydrodynamic self-diffusion of sedimenting non-Brownian spheres," *Phys. Fluids* **7**, 12 (1995).
- <sup>53</sup>E. Wacholder and N. F. Sather, "The hydrodynamic interaction of two unequal spheres moving under gravity through quiescent viscous fluid," *J. Fluid Mech.* **65**, 417 (1974).
- <sup>54</sup>R. Pesche, "Etude par simulation numérique de la segregation de particules dans une suspension bidisperse," Ph.D. thesis, Université de Nice-Sophia Antipolis, France (1998).
- <sup>55</sup>S. Dance and M. R. Maxey, "Incorporation of lubrication effects into the force coupling method for particulate two-phase flow," *J. Comput. Phys.* **189**, 212 (2003).
- <sup>56</sup>D. I. Dratler and W. R. Schowalter, "Dynamic simulation of suspensions of non-Brownian hard spheres," *J. Fluid Mech.* **325**, 53 (1996).
- <sup>57</sup>S. L. Dance, E. Climent, and M. R. Maxey, "Collision barrier effects on the bulk flow in a random suspension," *Phys. Fluids* **16**, 828 (2004).
- <sup>58</sup>F. R. Da Cunha and E. J. Hinch, "Shear-induced dispersion in a dilute suspension of rough spheres," *J. Fluid Mech.* **309**, 211 (1996).
- <sup>59</sup>M. P. Allen and D. J. Tildesley, *Computer Simulations of Liquids* (Oxford University Press, Oxford, 1987).
- <sup>60</sup>Y. Wang, R. Mauri, and A. Acrivos, "Transverse shear-induced liquid and particle tracer diffusivities of a dilute suspension of spheres undergoing a simple shear flow," *J. Fluid Mech.* **327**, 255 (1996).
- <sup>61</sup>A. Acrivos, G. K. Batchelor, J. Hinch, D. L. Koch, and R. Mauri, "The longitudinal shear-induced diffusion of spheres in a dilute suspension," *J. Fluid Mech.* **240**, 651 (1992).
- <sup>62</sup>G. P. Krishnan and D. T. Leighton, "Dynamic viscous resuspension of bidisperse suspensions," *Int. J. Multiphase Flow* **21**, 721 (1995).
- <sup>63</sup>M. Hoyos, J. C. Bacri, J. Martin, and D. Salin, "An study of the sedimentation of noncolloidal bidisperse concentrated suspensions by an acoustic technique," *Phys. Fluids* **6**, 3809 (1994).
- <sup>64</sup>M. A. Van der Hoef, R. Beestra, and J. A. Kuipers, "Lattice-Boltzmann simulations of low-Reynolds-number flows past mono- and bidisperse arrays of spheres: results for permeability and drag forces," *J. Fluid Mech.* **528**, 233 (2005).
- <sup>65</sup>R. H. Davis and N. A. Hill, "Hydrodynamic diffusion of a sphere sedimenting through a dilute suspension of neutrally buoyant spheres," *J. Fluid Mech.* **236**, 513 (1992).
- <sup>66</sup>H. Nicolai, Y. Peysson, and E. Guazzelli, "Velocity fluctuations of a heavy sphere falling through a sedimenting suspension," *Phys. Fluids* **8**, 855 (1996).
- <sup>67</sup>G. Bernard-Michel, A. Monavon, D. Lhuillier, D. Abdo, and H. Simon, "Particle velocity fluctuations and correlation lengths in dilute sedimenting suspensions," *Phys. Fluids* **14**, 2339 (2002).
- <sup>68</sup>A. J. C. Ladd, "Effects of container walls on the velocity fluctuations of

sedimenting spheres," *Phys. Rev. Lett.* **88**, 048301 (2002).

<sup>69</sup>R. G. Cox, "Instability of sedimenting bidisperse suspensions," *Int. J. Multiphase Flow* **16**, 617 (1990).

<sup>70</sup>P. M. Biesheuvel, H. Verweij, and V. Breedveld, "Evaluation of instability criterion for bidisperse sedimentation," *AIChE J.* **47**, 45 (2001).

<sup>71</sup>E. Climent, M. R. Maxey, and G. E. Karniadakis, "Dynamics of self-assembled chaining in magneto-rheological fluids," *Langmuir* **20**, 507 (2004).

<sup>72</sup>J. F. Brady and L. J. Durlofsky, "The sedimentation rate of disordered suspensions," *Phys. Fluids* **31**, 717 (1988).